Journal of Asian Earth Sciences: X 3 (2020) 100029

Contents lists available at ScienceDirect

Journal of Asian Earth Sciences: X

journal homepage: www.journals.elsevier.com/journal-of-asian-earth-sciences-x

Sr-Nd-Pb isotope systematics of fine sediments from the modern rivers in SW Japan: Implications for sediment provenance of the Northwest Pacific

Yu Saitoh[a,1,*], Masaharu Tanimizu[b], Tsuyoshi Ishikawa[c]

[a] Center for Advanced Marine Core Research, Kochi University, 200 Monobe Otsu, Nankoku, Kochi 783-8502, Japan
[b] Department of Applied Chemistry for Environment, School of Science and Technology, Kwansei Gakuin University, 2-1 Gakuen (Bdg. 7-3F), Sanda, Hyogo 669-1337, Japan
[c] Kochi Institute for Core Sample Research, Japan Agency for Marine-Earth Science and Technology (JAMSTEC), 200 Monobe Otsu, Nankoku, Kochi 783-8502, Japan

ARTICLE INFO

Keywords:
Sediment provenance
River sediment
Mud
Asian dust
Kuroshio Current
Southwest Japan

ABSTRACT

As reference data for comprehensive provenance analyses of deep-sea sediments in the Northwest Pacific region, we present Sr-Nd-Pb isotopic compositions of fine sediments sampled from 48 rivers in southwest Japan. Sr-Nd-Pb isotope ratios are reliable indicators of sediment sources. Although isotopic data of fine sediments in Chinese arid regions, known to be Asian dust sources, are abundant, comparable data from southwest Japan are scarce, even though southwest Japan, owing to its tectonic activity, is a major sediment source to the Northwest Pacific. Sr-Nd-Pb isotope ratios of our riverine fine sediment samples vary greatly ($^{87}Sr/^{86}Sr$, 0.707–0.724; $^{143}Nd/^{144}Nd$, 0.5120–0.5129; $^{206}Pb/^{204}Pb$, 18.16–18.89; $^{207}Pb/^{204}Pb$, 15.55–15.66; and $^{206}Pb/^{204}Pb$, 38.13–39.09), and these variations are clearly dependent on the principal geology of each river's watershed. These results indicate that these isotope ratios can be effectively used to discriminate the geological sources of the sediments. Sediments from watersheds dominated by Quaternary volcanic rocks have the lowest $^{87}Sr/^{86}Sr$ and Pb isotope ratios and the highest $^{143}Nd/^{144}Nd$ ratios, whereas sediments from watersheds dominated by accretionary sedimentary rocks generally have high $^{87}Sr/^{86}Sr$ and Pb isotope ratios and low $^{143}Nd/^{144}Nd$ ratios, but their specific values vary depending on the age and geographic location of the rocks. The isotope compositions of sediments from watersheds with exposed Cretaceous granitic and metamorphic rocks are also distinctive. Comparison between the isotope ratios of Japanese river sediments and the Northwest Pacific seafloor sediments suggests the importance of sediment transport by the Kuroshio Current to the Northwest Pacific.

1. Introduction

Tracing sediment particles can yield many clues to help us understand weathering, atmospheric and oceanic circulation, and plate tectonics. Elucidating the origins of sediment particles accumulated in various environments can provide insights into earth surface processes. Understanding the origin of particles in deep-sea sedimentary successions is particularly valuable because they record a continuous history of the surface processes that contributed to their accumulation (e.g., Lamy et al., 2001; Saitoh et al., 2015; Schindlbeck et al., 2018; Stumpf et al., 2011; van der Lubbe et al., 2016).

In deep-sea sediments of the North Pacific (Fig. 1A), the detrital silicate fraction has been generally interpreted to be of aeolian origin (e.g., Hovan et al., 1991; Rea et al., 1985; Uematsu et al., 1983; Windom, 1969), and, on this basis, it has been used to infer Cenozoic climatic and tectonic conditions in and around the North Pacific region. For example, Rea et al. (1998) related an increase of the mass accumulation rate at 3.6 Ma, observed at Ocean Drilling Program (ODP) site 885/886 in the central North Pacific, to an increase of aridity in dust source regions caused by uplift of the Tibetan Plateau. Similarly, Li et al. (2011) attributed a decrease of the $^{143}Nd/^{144}Nd$ ratio of sediments from core LL44-GPC3 from the central North Pacific reported by Pettke et al. (2002) to an increased contribution of sediments from the north Tibetan Plateau to arid region dust sources in relation to modeled elevation changes of the plateau after 15 Ma. In contrast, particle transport by ocean-surface circulation to the North Pacific has been almost ignored. Fine particles are generally assumed to become incorporated into fecal pellets by zooplankton and then to rapidly settle out of the water column in coastal areas (Honjo et al., 1982; Rea et al., 1985; Scheidegger and Krissek, 1982).

Only a few studies have examined transport of terrigenous material by ocean currents (e.g., Ehlert and Frank, 2011; Franzese et al., 2009;

* Corresponding author.
E-mail address: yu-saitoh@aoni.waseda.jp (Y. Saitoh).
[1] Present address: Department of Earth Sciences, Resources and Environmental Engineering, Waseda University, 3-4-1 Okubo, Shinjuku-ku, Tokyo 169-8555, Japan

https://doi.org/10.1016/j.jaesx.2020.100029
Received 14 October 2019; Received in revised form 20 April 2020; Accepted 20 April 2020
Available online 03 May 2020

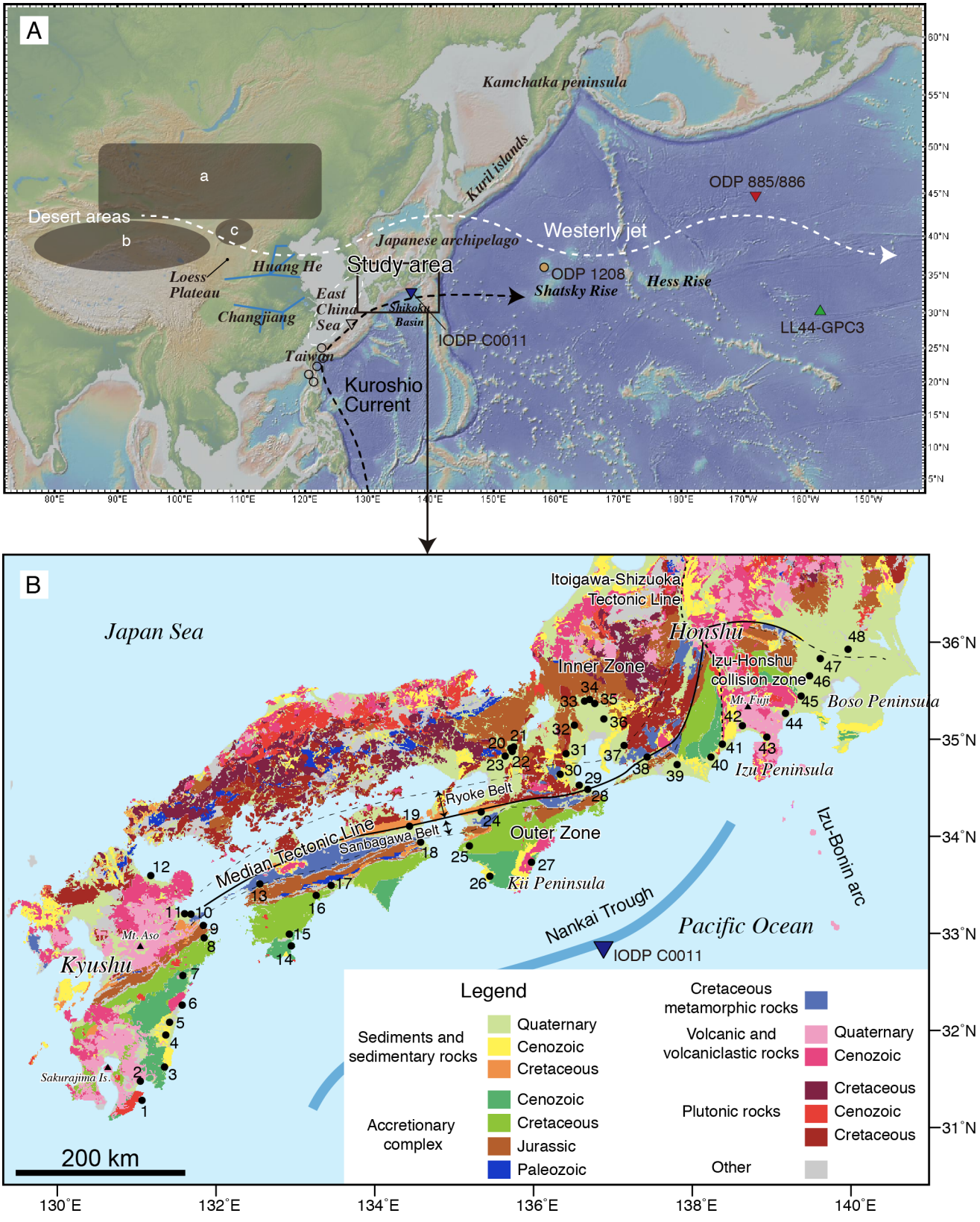

Fig. 1. A. Location of the study area, drilling sites of the ocean-floor sediments compared with the results of this study, possible sources of Asian dust (desert areas a: on the northern boundary of China, b: on the northern margin of Tibetan Plateau, and c: on the Ordos Plateau, and the Loess Plateau), and fluvial sources in relation to the path ways of the westerly jet (white dashed line) and the Kuroshio Current (black dashed line). B. River sediment sampling sites and the distribution of geological units in southwest Japan (modified after Geological Survey of Japan, AIST (2015)).

Underwood and Fergusson, 2005). Because fluvial inputs from East and Southeast Asia to the Pacific are huge (e.g., Wang et al., 2011), the Kuroshio Current (KC), one of the strongest western boundary currents in the world, is expected to transport considerable amounts of fine particles long distances. For example, Dou et al. (2012) reported that Holocene fine sediments in the center of the Okinawa trough in the East China Sea (ECS) are dominated by mineral particles derived from Taiwan and transported by the KC. Furthermore, most upper Cenozoic hemipelagic sediments on the northernmost Philippine Sea plate consist of detrital grains derived from land areas around the ECS and transported by the KC (Saitoh et al., 2015). The importance of particle transport by the KC is also suggested by the occurrence of pollen and spores derived from Japan and the area around the ECS in sediments on the Hess Rise, a seamount located far to the east of Japan (Kawahata and Ohshima, 2002). Determination of whether the long-distance transport of sediments by the KC contributes substantially to deposition in the North Pacific is thus critical for interpreting the origin of sediments in the Northwest Pacific.

The radiogenic isotopic signatures of Sr, Nd, and Pb of pelagic and hemipelagic sediments in the North Pacific have been well investigated with the aim of estimating the Asian dust contribution to those sediments (e.g., Asahara, 1999; Jones et al., 2000; Nakai et al., 1993; Pettke et al., 2000). Isotope ratios of Sr, Nd, and Pb are widely accepted as reliable provenance tracers of fine sediments (e.g., Dou et al., 2012; Franzese et al., 2006; Grousset et al., 1992) because Sr-Nd-Pb isotope ratios of the silicate components of sediments vary widely, depending on the type and age of the source rocks, and their values are well preserved during transportation (e.g., Grousset and Biscaye, 2005).

As a fingerprint of dust sources, Sr-Nd-Pb isotope ratios of sediments in the arid areas of North China, including the Taklimakan desert and the Gobi (stony desert), have been well investigated (Chen et al., 2007; Nakano et al., 2004; Sun, 2005; Sun and Zhu, 2010), but Sr-Nd-Pb isotopic data of terrestrial sediment sources for the KC are scarce; in particular, data from southwest Japan, the last land area along the KC path before the current turns eastward as the Kuroshio Extension, are lacking.

In this study, our aim was to compile a comprehensive database of Sr-Nd-Pb isotope ratios of fine sediments from rivers in southwest Japan to improve the resolution of provenance analyses of fine particles in the Northwest Pacific. Southwest Japan is expected to be a major source of sediments to the Northwest Pacific because of the active late Cenozoic uplift of the region. In fact, late Holocene denudation rates in the mountains of Japan are among the highest in the world (Korup et al., 2014). In addition, various kinds of rocks, including sedimentary, metamorphic, plutonic, and volcanic rocks, are distributed in the land areas of the southwest Japan arc. Thus, large amounts of sediments with a wide range of isotopic variation are expected to be discharged by rivers in southwest Japan into the northwest Pacific. Nevertheless, few studies have reported radiogenic isotopic ratios of Japanese sediments (e.g., Jomori et al., 2013). Therefore, our aim in this study is to assess the Sr-Nd-Pb isotopic variation of fine sediments in southwest Japan comprehensively for the first time, and then to compare the Sr-Nd-Pb isotopic ratios of those sediments with reported data for North Pacific deep-sea sediments.

Another study aim is to provide information useful in considering the formation history of the Japanese archipelago, an island arc system developed at a typical convergent margin, by investigating the relationships between the isotope ratios of fine river sediments and the geology of the river watersheds in southwest Japan. The sedimentary isotopic data obtained by this study are expected to reflect the general characteristics of the geological units distributed in the river watersheds because river sediments result from the thorough sampling of clastics produced in the watershed by natural processes. In addition, we avoided biases in the mineralogy caused by hydraulic sorting during sediment transport (Garcia et al., 2004; Garzanti et al., 2008) because we targeted solely the fine sediment fraction that is transported in suspension by the rivers. Therefore, we obtained highly representative isotopic composition data for watershed geology in this study; we expect these data to be useful for deciphering the isotopic relationships among widely distributed geological units in southwest Japan.

2. Geology of southwest Japan

In this paper, we refer to the part west of Boso peninsula in the Japanese archipelago as Southwest Japan (Fig. 1B). The Japanese archipelago has evolved since the Permian Period by means of the subduction of several oceanic plates beneath the ancient Eurasian continent (Taira, 2001). As a result, the basement rocks of Japan are composed mainly of Jurassic to Paleogene accretionary prisms (Fig. 1B). These prisms are composed in turn of various kinds of sedimentary, metamorphic, and basaltic rocks. In addition, Cretaceous to Paleogene granitic rocks that have intruded into the prisms are widely exposed in southwest Japan, and Neogene to Quaternary volcanic rocks cover a considerable portion of eastern Honshu Island and parts of both northern and southern Kyushu Island.

The Median Tectonic Line (MTL) is a giant strike-slip fault that cuts the southwest Japan arc longitudinally, dividing it into two main parts (Fig. 1B), an Inner Zone to the north of the MTL and an Outer Zone to its south. The present-day active MTL fault zone is inferred to be a dextral strike-slip fault associated with the oblique subduction of the Philippine Sea plate since 5–6 Ma (Kamata and Kodama, 1994; Sugiyama, 1994).

Accretionary complex bands have an east–west orientation in southwest Japan. The rocks of the accretionary prisms are classified into three groups according to the period during which they accreted: Jurassic, Cretaceous, or Paleogene. Accretionary prism rocks accreted during the Jurassic are composed of Carboniferous–Permian basaltic rocks, Carboniferous–Permian–Triassic reef limestones, Permo-Triassic cherts and shales, and Jurassic turbidites (e.g., Matsuoka, 1992; Nakae, 2000). These Jurassic accretionary complexes are distributed in both the Inner and Outer zones, whereas Cretaceous and Paleogene accretionary complexes occur only in the Outer Zone.

Two contrasting Cretaceous metamorphic belts are juxtaposed across the MTL. The Ryoke Belt, which is distributed north of the MTL, was metamorphosed under low-pressure, high-temperature conditions, and is associated with large amounts of granitic rocks, whereas the Sanbagawa Belt, which is distributed south of the MTL, was metamorphosed under high-pressure, low-temperature conditions (Miyashiro, 1961). The rocks of both metamorphic belts are mainly derived from Jurassic to Lower Cretaceous accretionary prism rocks (Isozaki and Itaya, 1990; Nakajima, 1994; Okamoto et al., 2000), and the metamorphism of both belts occurred during the Cretaceous (e.g., Nakajima, 1994). The juxtaposition of these two belts reflecting quite different metamorphic conditions suggests that hundreds of kilometers of left-lateral motion occurred along the MTL during the Cretaceous Period (e.g., Brown, 2010; Sakashima et al., 2003; Tazawa, 2000).

Cretaceous granitic rocks are widely distributed in the Inner Zone. In the studied watersheds, most of these granitic rocks are in the Ryoke Belt. The isotopic ages of both the granitic and metamorphic rocks of the Ryoke Belt become younger eastward, which suggests that the area of active magmatism and metamorphism shifted eastward from Kyushu toward central Japan between 105 and 65 Ma (Nakajima, 1994). Subduction of the Izanagi–Pacific ridge, which was directed parallel or subparallel to the coastline of ancient southwest Japan, beneath the Eurasian plate may have caused the late Cretaceous granitic magmatism in southwest Japan (Uyeda and Miyashiro, 1974).

Active volcanism since the Miocene resulted in the eruption of substantial amounts of volcanic and volcaniclastic rocks around the Izu-Honshu collision zone in central Japan and the Kyushu arc.

Cenozoic sedimentary rocks that occur locally in southwest Japan include forearc-basin fill sediments (e.g., Miyazaki Group, Kakegawa Group) and fluvial or lacustrine sediments (e.g., Kobiwako Group,

Tokai Group).

Sediments eroded from the various rocks described above are discharged to the sea through densely developed river systems in Southwest Japan. This region is characterized by a temperate humid climate. The annual precipitation ranges from 1000 to 3000 mm, and the annual discharges of the major 19 rivers in this region, of which drainages exceed 1000 km^2 in area, range from 30 to about 300 $m^3\ s^{-1}$. The annual sediment discharge of the Tenryu River (no. 39, Fig. 1B), which is one of largest rivers in Southwest Japan having drainage of 5090 km^2 in area, is estimated to be about 1–3 $\times$ 10^6 $m^3\ yr^{-1}$ (Huang, 2011 and references therein).

3. Materials and methods

3.1. Sampling

One hundred and two sediment samples in total were collected during the period between November 2014 and July 2015 from along the lower courses of 48 rivers in southwest Japan that flow into the Pacific Ocean (Fig. 1B). The watersheds of these rivers collectively include most of the major lithologies of central and western Japan. Sampling sites were located well upstream of the estuarine basin of rivers. We collected more than one sample from most rivers except for rivers of nos. 1, 14, 21, 25, 38, and 44 in order to ensure the representativeness of the results of analysis. Scoops used in sampling were carefully washed with river water of each site before sampling to avoid contamination with samples from other sites.

We sampled undisturbed silty sediments that, as indicated by sedimentological and geomorphological observations, could be regarded as having been transported by the river flow as a homogeneous suspended load. For example, muddy sediments deposited in depressions in backwater or inactive channels, and mud drapes on sand dunes formed during floods were selected. Because the behavior of sediment particles depends on their settling velocity (Garzanti et al., 2008; Morton and Hallsworth, 1999), the mineralogical composition of the deposited sediments depends not only on the composition of the source rocks but also on the depositional process. This hydrological bias is smaller, however, for silt-sized grains, because their settling is resisted chiefly by fluid viscosity, compared with sand and pebbles, the settling of which is governed largely by turbulent effects (Garzanti et al., 2008). Therefore, muddy sediments are expected to reflect the characteristics of source rocks more straightforwardly than coarser sediments.

The composition of surface geology composition in the watershed of each sampled river was calculated in the ESRI ArcGIS software environment by overlaying geologic map data provided by the Geological Survey of Japan, AIST (2015) (Fig. 1B) on watershed boundaries extracted from topographic maps.

3.2. Analytical procedures

3.2.1. Sample pretreatment

Even though the muddy sediments for sampling were carefully selected in the field, natural sediments generally contain grains covering a wide size range. To minimize the effect of grain size on the isotopic composition of sediments (Feng et al., 2009; Mayer et al., 2011), particles smaller than 20 μm in diameter were extracted for analysis by using their different settling velocity in water. This size fraction was chosen because it is equivalent to the grain size of the hemipelagic sediments that are widely distributed in the Shikoku Basin (Saitoh, 2014). About 500 mg of samples were well shaken with 13–14 mL of ultrapure water in a polypropylene tube of 15 mm in diameter and 12 cm in height. After the tube was left stand for 13 min, 10 mL of the supernatant, in which the target size fraction was contained theoretically, was recovered. Adding 10 mL of ultrapure water to the residue, this process was repeated 4 or 5 times until the supernatant becomes clear. Then the all recovered supernatants were combined in a precleaned bottle and well stirred to homogenize. Actual grain-size distribution in this target fraction of each sample was then analyzed by using a Malvern Mastersizer 2000 laser diffractometer with an automated sample dispersion unit (Hydro 2000S) at the Kochi Core Center (KCC), Nankoku, Japan, and confirmed that the 90-percentile diameter fitted inside 16 $\pm$ 5 (2σ) μm (Table A.1).

Because materials adsorbed onto particle surfaces, carbonate components, and Fe-Mn hydroxides can greatly affect the chemical and isotopic composition of sediment samples, we removed these components following the method used by previous provenance studies (e.g., Asahara et al., 1995; Bentahila et al., 2008; Sun, 2005). Dried sample (200–300 mg) was leached with 1 M HCl at room temperature for 1 day and then centrifuged for 10 min at 3000 rpm, after which the supernatant was removed and the residue was cleaned with ultrapure water. This rinsing procedure was performed four times. After the final centrifuging, the supernatant was removed and the residue was dried at 105 °C for 1 day. The dried residues were thoroughly powdered and homogenized in agate mortars and used for the chemical and isotope analyses in this study.

3.2.2. Measurements

About 100 mg of each sample was completely digested in a concentrated HF–$HClO_4$–HNO_3 solution in tightly stoppered Teflon vials on a hot plate at 180 °C for 2–3 days. The digested solution was evaporated to dryness and then dissolved in 2 mL of 2 M HNO_3. Next, a 50-μL subsample of the 2 mL sample solution was evaporated to dryness and re-dissolved in 5 mL of 0.15 M HNO_3 for elemental analysis. The rest of the sample solution was used for Sr-Nd-Pb isotopic analyses.

Concentrations of Sr, Nd, and Pb were measured with an inductively coupled plasma mass spectrometer (ELAN DRC II, PerkinElmer Inc.) installed at the KCC. The results were corrected for instrumental drift and any sample-originated matrix effect by using an internal standard. All reagents were high-purity grade, and the blank contribution to the analytical response was ≪1%.

Sr and Pb were separated from each sample solution by using a column filled with 0.2 mL Sr resin (Eichrom Technologies Inc.). The Sr fraction was collected by using 2 mL of 0.05 M HNO_3 after elution of the other elements with 2 mL of 6 M HNO_3 followed by 1 mL of 3 M HNO_3. Next, Pb fractions were collected with 3 mL of 6 M HCl. Nd was separated from the sample solution remaining after the separation of Sr and Pb first by using a column filled with 1 mL of cation exchange resin (AG50W-X12, Bio-Rad Laboratories Inc.). Then, the rare earth element (REE) fraction, including Nd, was collected with 7 mL of 6 M HNO_3 after elution of other elements with 2 mL of 2.5 M HCl followed by 11 mL of 2.5 M HNO_3. Next, Nd was separated from the REE fraction by using a column filled with 2 mL Ln resin (Eichrom Technologies Inc.). The Nd fraction was collected with 8 mL of 0.25 M HCl after elution of other elements with 8 mL of 0.25 M HCl.

Sr and Nd isotope ratios were measured by using a Triton thermal ionization mass spectrometer (Thermo Fisher Scientific Inc.) installed at the KCC. Measured $^{87}Sr/^{86}Sr$ and $^{143}Nd/^{144}Nd$ isotope ratios were normalized with respect to $^{86}Sr/^{88}Sr$ = 0.1194 and $^{146}Nd/^{144}Nd$ = 0.7219, respectively. Repeated analyses of the standard samples NIST SRM 987 and JNdi-1 yielded an average $^{87}Sr/^{86}Sr$ value of 0.710241 $\pm$ 0.000012 (2σ) (n = 28) and $^{143}Nd/^{144}Nd$ value of 0.512109 $\pm$ 0.000012 (2σ) (n = 23), respectively. Sr and Nd isotope ratios of the samples were corrected with respect to standard values $^{87}Sr/^{86}Sr$ = 0.710250 (NIST SRM 987) and $^{143}Nd/^{144}Nd$ = 0.512115 (JNdi-1) (Tanaka et al., 2000), respectively. Pb isotope ratios were measured by using a multiple collector inductively coupled plasma mass spectrometer (Neptune, Thermo Fisher Scientific Inc.) installed at the Research Institute for Humanity and Nature, Kyoto, Japan (sample nos. 1–35) or at the KCC (sample nos. 36–102) by the Tl-spike method (Tanimizu and Ishikawa, 2006). All measurements were corrected with respect to the NIST SRM 981 standard values $^{206}Pb/^{204}Pb$ = 16.9308, $^{207}Pb/^{204}Pb$ = 15.4839, and $^{208}Pb/^{204}Pb$ = 36.6743 (Tanimizu and

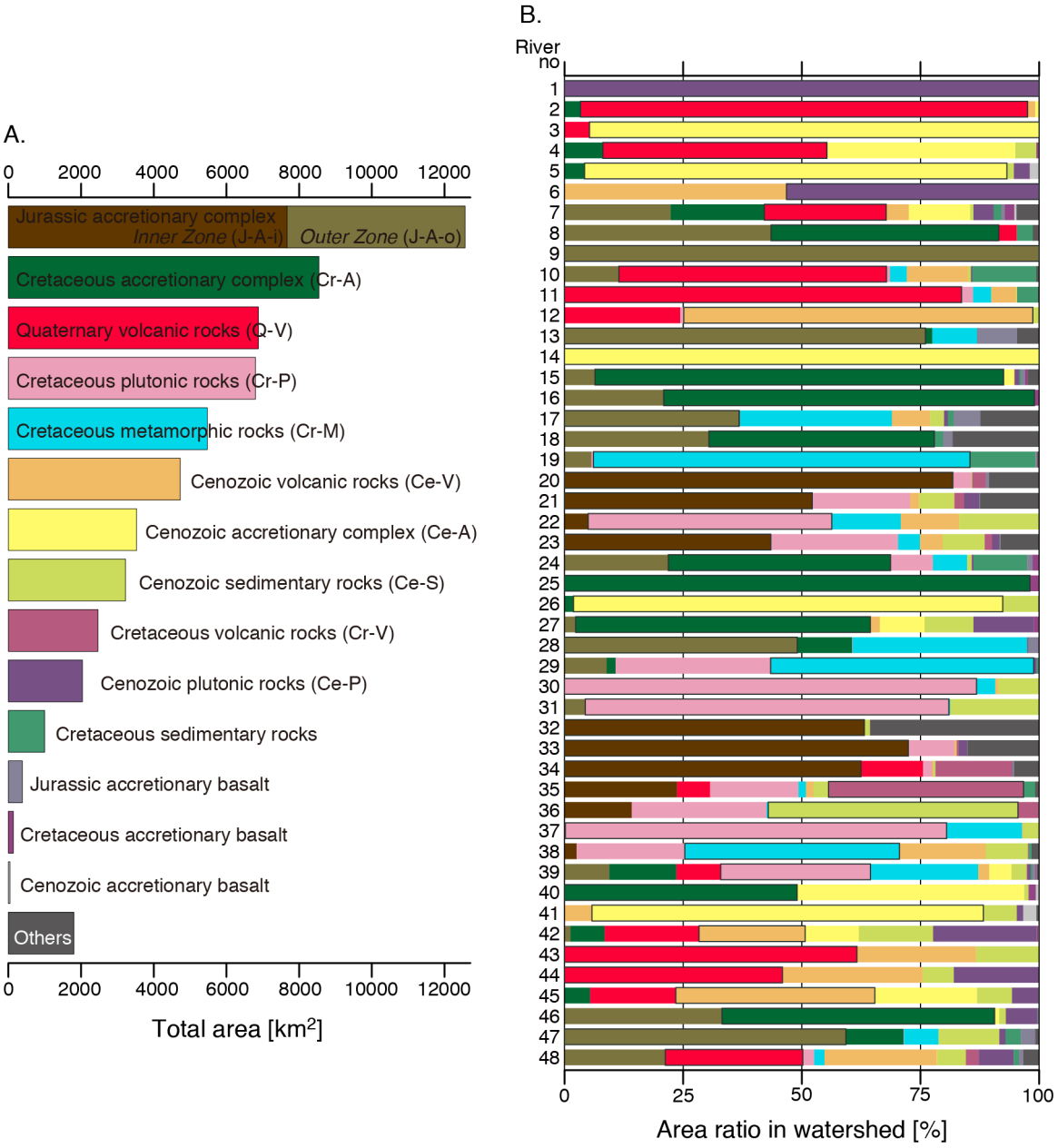

Fig. 2. A. Total exposed area of geological units in all watersheds. B. Geological composition of the rocks exposed in each watershed. Colors are as shown in panel A.

Ishikawa, 2006).

4. Results

4.1. Geological composition of the watersheds

The total exposed area of each geological unit in all 48 watersheds and the areal proportion of each unit within each watershed determined by using ESRI ArcGIS software are shown in Fig. 2. Quaternary sediments were excluded from these calculations because most of them are alluvial plain and terrace deposits, which we considered to correspond to modern river sediments. We classified the principal geology of each of the 48 watersheds into one of 10 categories: a Jurassic, Cretaceous, or Cenozoic accretionary complex (J-A, Cr-A, Ce-A, respectively); Cretaceous or Cenozoic plutonic rocks (Cr-P, Ce-P, respectively); Cretaceous, Neogene, or Quaternary volcanic (lastic) rocks (Cr-V, Ce-V, Q-V, respectively); Cretaceous metamorphic rocks (Cr-M); or Cenozoic sedimentary rocks (Ce-S). In determining the area occupied by the accretionary complexes, accretionary basalts were excluded, because they occupy a limited area and are of an essentially different lithology from the complexes, owing to their igneous origin. If all 48 watersheds are considered in aggregate (Fig. 2A), surface exposures of J-A account for the largest areal proportion; about 61% of the total J-A area is in the Inner Zone (J-A-i), and 39% is in the Outer Zone (J-A-o). Surface exposures of Cr-A, Q-V, Cr-P, and Cr-M, in that order, are next in areal dominance.

Hereinafter, for convenience, river sediments from a watershed dominated by a specific geology are identified by simply prefixing the abbreviation for the principal geology to the word “sediments”. For example, “Q-V sediments” means “sediments from rivers with a watershed dominated by Quaternary volcanic (lastic) rocks”.

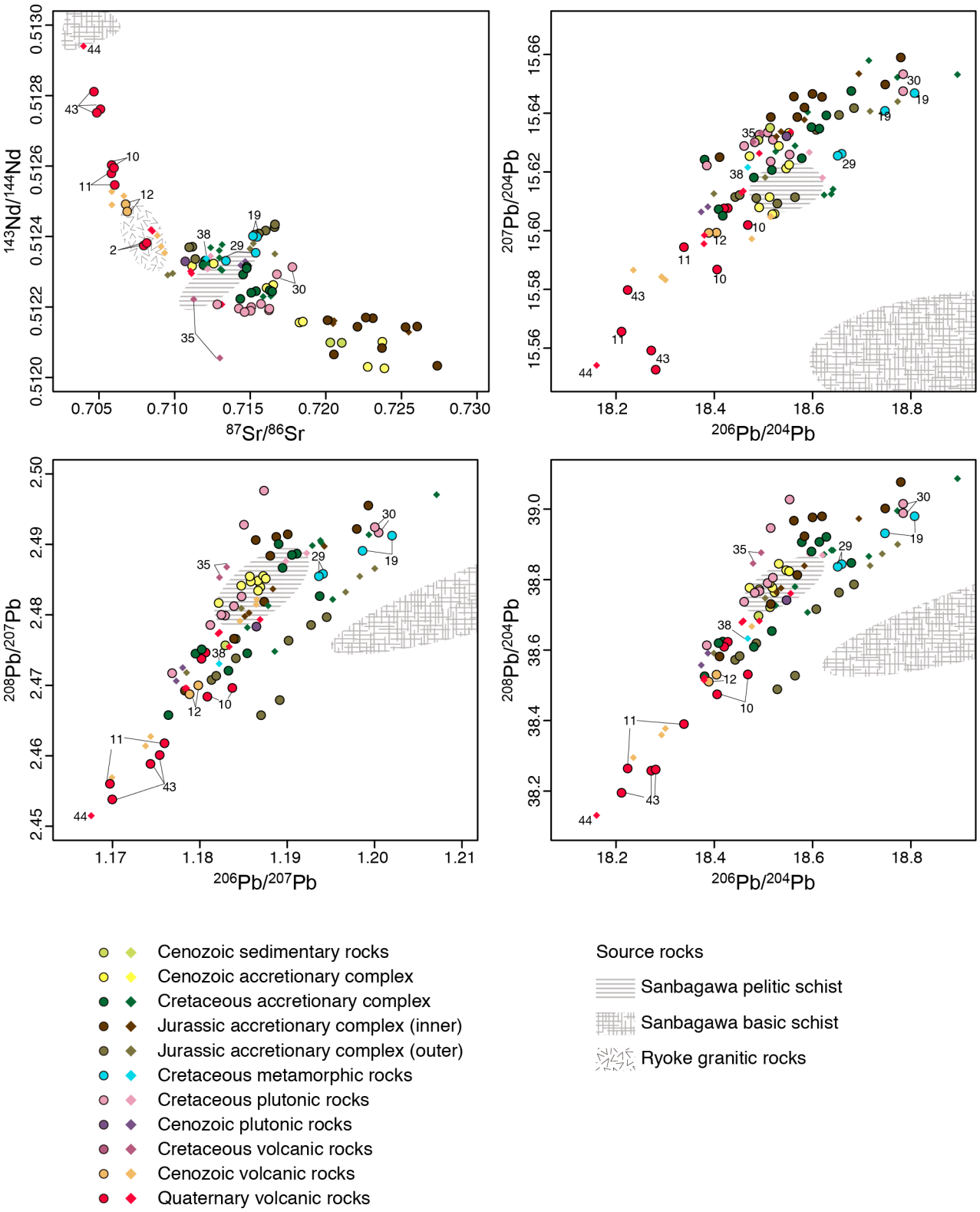

Fig. 3. Relationships among Sr, Nd, and Pb isotope ratios of the fine fraction (< 20 μm) of river sediments in relation to those of some possible source rocks (Ryoke granitic rocks: Kagami et al., 1992; Okano et al., 2000; Sanbagwa metamorphic rocks: Uno et al., 2014). Plots are color-coded according to the principal geological unit in each river's watershed. Symbol shape indicates the proportion of the principal geological unit in the watershed: circle, > 50%; diamond, < 50%. River numbers mentioned in the main text are indicated.

4.2. Sr-Nd-Pb isotope ratios of river sediments in southwest Japan

The Sr-Nd-Pb isotope ratios of the river sediment samples vary widely (Fig. 3 and Table 1), as expected given the heterogeneous geology of southwest Japan.

Q-V sediments, which are characterized by low $^{87}Sr/^{86}Sr$ (0.704–0.708), high $^{143}Nd/^{144}Nd$ (0.5124–0.5129), and generally low Pb isotope ratios ($^{206}Pb/^{204}Pb$ = 18.2–18.5; $^{207}Pb/^{204}Pb$ = 15.55–15.61;

Table 1
Isotope ratios and concentrations of Sr, Nd, and Pb in the fine fraction of river sediments in southwest Japan.

River no.	River name	Sample no.	$^{87}Sr/^{86}Sr$	$^{143}Nd/^{144}Nd$	$^{*206}Pb/^{204}Pb$	$^{*207}Pb/^{204}Pb$	$^{*208}Pb/^{204}Pb$	Sr (mg/kg)	Nd (mg/kg)	Pb (mg/kg)
1	Hirose	1	0.710700 ± 4	0.512329 ± 4	18.5471 ± 2	15.6321 ± 2	38.7415 ± 6	45.6	3.1	20.0
2	Hishida	2	0.707953 ± 4	0.512375 ± 4	18.4274 ± 2	15.6076 ± 2	38.6234 ± 6	65.2	6.2	9.0
		3	0.708161 ± 5	0.512382 ± 4	18.4199 ± 1	15.6076 ± 1	38.6094 ± 5	48.1	6.4	7.7
3	Saketani	4	0.718262 ± 5	0.512156 ± 5	18.5463 ± 2	15.6212 ± 2	38.8267 ± 6	43.0	4.5	7.4
		5	0.718480 ± 4	0.512158 ± 4	18.5522 ± 3	15.6224 ± 3	38.8238 ± 7	41.7	3.1	7.8
4	Oyodo	6	0.714725 ± 4	0.512192 ± 4	18.5554 ± 2	15.6336 ± 2	38.7608 ± 5	46.8	3.6	10.8
		7	0.713122 ± 4	0.512208 ± 4	18.4916 ± 2	15.6263 ± 2	38.6826 ± 6	54.7	3.9	11.6
5	Hitotsuse	8	0.722772 ± 5	0.512030 ± 4	18.5516 ± 2	15.6333 ± 2	38.8240 ± 6	41.0	9.4	9.1
		9	0.723871 ± 5	0.512026 ± 4	18.5312 ± 2	15.6288 ± 2	38.8447 ± 5	29.9	4.3	8.5
6	Tsuno	10	0.714666 ± 4	0.512329 ± 3	18.3735 ± 2	15.6064 ± 2	38.5573 ± 6	27.2	3.3	15.0
		11	0.714376 ± 4	0.512318 ± 4	18.3869 ± 2	15.6081 ± 2	38.5912 ± 5	32.5	10.2	14.6
7	Gokase	12	0.711060 ± 4	0.512301 ± 4	18.4560 ± 2	15.6130 ± 2	38.6786 ± 6	93.8	8.3	18.9
		13	0.711119 ± 5	0.512295 ± 4	18.4592 ± 2	15.6135 ± 2	38.6827 ± 7	95.0	7.9	18.6
8	Banjo	14	0.716364 ± 5	0.512231 ± 4	18.7145 ± 3	15.6580 ± 3	38.8660 ± 7	50.5	2.6	10.6
		15	0.715854 ± 4	0.512229 ± 4	18.5898 ± 2	15.6404 ± 2	38.7070 ± 7	58.1	3.5	11.3
9	Aoe	16	0.716612 ± 5	0.512427 ± 5	18.5643 ± 3	15.6114 ± 3	38.5274 ± 7	25.3	3.9	10.4
		17	0.716631 ± 5	0.512434 ± 4	18.5282 ± 2	15.6092 ± 2	38.4887 ± 6	22.1	3.0	10.8
10	Ono	18	0.705835 ± 4	0.512603 ± 4	18.4683 ± 2	15.6019 ± 2	38.5309 ± 7	104.6	7.4	12.9
		19	0.705992 ± 5	0.512595 ± 5	18.4058 ± 2	15.5868 ± 2	38.4743 ± 6	90.8	6.4	9.7
11	Oita	20	0.706042 ± 5	0.512546 ± 5	18.2238 ± 3	15.5798 ± 3	38.2641 ± 8	103.9	7.4	14.5
		21	0.705817 ± 4	0.512579 ± 4	18.3382 ± 2	15.5944 ± 2	38.3899 ± 7	103.6	5.2	14.5
12	Yamakuni	22	0.706766 ± 5	0.512492 ± 5	18.4045 ± 2	15.5993 ± 2	38.5303 ± 7	79.0	7.5	7.2
		23	0.706868 ± 4	0.512471 ± 5	18.3888 ± 2	15.5992 ± 2	38.5105 ± 6	76.4	7.9	7.0
13	Hiji	24	0.716021 ± 5	0.512417 ± 5	18.6074 ± 2	15.6343 ± 2	38.7161 ± 6	38.2	9.4	7.8
		25	0.715574 ± 5	0.512409 ± 5	18.6537 ± 2	15.6394 ± 2	38.7633 ± 6	42.1	10.0	7.6
		26	0.715285 ± 4	0.512405 ± 5	18.6843 ± 2	15.6417 ± 2	38.7864 ± 6	45.8	10.6	7.5
14	Shimonokae	27	0.723732 ± 4	0.512101 ± 4	18.4717 ± 2	15.6254 ± 2	38.7770 ± 5	23.8	7.2	8.6
15	Shimanto	28	0.715385 ± 4	0.512245 ± 5	18.6279 ± 2	15.6393 ± 2	38.9212 ± 7	68.3	16.0	5.8
		29	0.716285 ± 8	0.512247 ± 5	18.5976 ± 2	15.6352 ± 2	38.8797 ± 5	55.8	13.5	6.0
		30	0.716448 ± 4	0.512244 ± 4	18.6137 ± 2	15.6347 ± 2	38.9070 ± 6	54.4	13.3	6.2
16	Shinjo	31	0.715064 ± 5	0.512241 ± 4	18.6787 ± 2	15.6476 ± 2	38.8475 ± 6	65.3	11.5	7.9
		32	0.714344 ± 4	0.512223 ± 5	18.3803 ± 2	15.6242 ± 2	38.5258 ± 7	57.1	7.0	8.7
17	Niyodo	33	0.715206 ± 5	0.512380 ± 4	18.7416 ± 3	15.6401 ± 3	38.8731 ± 7	58.7	14.7	6.5
		34	0.716630 ± 5	0.512351 ± 5	18.7171 ± 3	15.6407 ± 2	38.8394 ± 7	52.9	14.1	7.0
		35	0.714986 ± 4	0.512365 ± 5	18.7731 ± 2	15.6440 ± 2	38.8999 ± 6	59.5	14.4	6.3
18	Naka	36	0.712965 ± 5	0.512340 ± 4	18.8949 ± 2	15.6532 ± 2	39.0867 ± 5	124.0	20.7	6.7
		37	0.712153 ± 6	0.512321 ± 4	18.7724 ± 2	15.6522 ± 2	38.9954 ± 6	142.6	20.1	7.9
19	Yoshino	38	0.715458 ± 5	0.512399 ± 5	18.8076 ± 2	15.6468 ± 2	38.9800 ± 6	63.1	14.2	6.0
		39	0.715179 ± 6	0.512401 ± 4	18.7474 ± 2	15.6408 ± 2	38.9313 ± 5	66.7	13.3	6.3
20	Katsura	40	0.725274 ± 6	0.512143 ± 6	18.4107 ± 2	15.6250 ± 2	38.5819 ± 5	50.6	18.0	18.8
		41	0.726044 ± 6	0.512145 ± 6	18.5149 ± 2	15.6387 ± 2	38.7307 ± 5	43.4	11.4	15.0
21	Uji	42	0.722089 ± 6	0.512144 ± 4	18.5689 ± 2	15.6387 ± 2	38.8131 ± 5	57.3	21.6	17.8
22	Kizu	43	0.716238 ± 6	0.512191 ± 6	18.5085 ± 2	15.6334 ± 2	38.7901 ± 6	40.5	3.8	11.7
		44	0.716266 ± 6	0.512195 ± 4	18.4919 ± 2	15.6327 ± 1	38.7674 ± 4	51.0	13.2	13.2
		45	0.715709 ± 5	0.512209 ± 5	18.5192 ± 2	15.6309 ± 2	38.8055 ± 6	51.8	11.0	12.8
23	Yodo	46	0.720546 ± 5	0.512161 ± 5	18.5358 ± 2	15.6338 ± 2	38.7759 ± 6	61.5	18.8	13.6
		47	0.720475 ± 6	0.512153 ± 5	18.5834 ± 2	15.6378 ± 2	38.8390 ± 6	61.1	18.1	12.5
		48	0.720339 ± 6	0.512164 ± 5	18.5264 ± 2	15.6320 ± 2	38.7641 ± 6	59.2	17.8	15.8
		49	0.725479 ± 6	0.512129 ± 4	18.6941 ± 2	15.6534 ± 2	38.9729 ± 5	48.3	14.4	12.5
24	Ki	50	0.713039 ± 6	0.512307 ± 5	18.5643 ± 2	15.6289 ± 2	38.7799 ± 5	85.5	12.3	7.2
		51	0.713142 ± 6	0.512304 ± 5	18.5249 ± 2	15.6269 ± 2	38.7266 ± 5	85.2	13.7	9.1
25	Hidaka	52	0.714529 ± 6	0.512292 ± 4	18.5780 ± 2	15.6247 ± 2	38.9062 ± 6	85.7	28.5	8.5
26	Hiki	53	0.716521 ± 6	0.512262 ± 5	18.5125 ± 2	15.6114 ± 2	38.7900 ± 5	71.2	21.8	7.8
		54	0.716082 ± 6	0.512254 ± 5	18.4914 ± 2	15.6079 ± 2	38.7724 ± 5	86.1	24.5	9.1
27	Kumano	55	0.714776 ± 5	0.512314 ± 4	18.4087 ± 3	15.6073 ± 3	38.6200 ± 10	82.4	22.3	13.3
		56	0.714769 ± 5	0.512310 ± 5	18.4174 ± 3	15.6051 ± 3	38.6242 ± 9	79.4	24.8	13.4
28	Miya	57	0.709872 ± 5	0.512295 ± 5	18.3992 ± 5	15.6126 ± 5	38.5913 ± 12	79.0	10.7	7.8
		58	0.709544 ± 4	0.512291 ± 6	18.5036 ± 8	15.6181 ± 7	38.7474 ± 20	171.5	14.7	9.9
29	Kushida	59	0.713386 ± 4	0.512331 ± 5	18.6592 ± 5	15.6262 ± 4	38.8438 ± 11	93.8	12.5	7.9
		60	0.715359 ± 5	0.512354 ± 15	18.6511 ± 6	15.6256 ± 5	38.8369 ± 16	87.2	14.8	10.0
30	Kumode	61	0.717789 ± 4	0.512313 ± 4	18.7843 ± 4	15.6475 ± 4	38.9884 ± 14	79.4	17.2	9.0
		62	0.716766 ± 5	0.512293 ± 4	18.7843 ± 4	15.6533 ± 4	39.0150 ± 12	109.4	19.7	9.6
31	Suzuka	63	0.712825 ± 4	0.512207 ± 5	18.5148 ± 4	15.6235 ± 4	38.9463 ± 11	130.2	25.2	13.3
		64	0.714247 ± 4	0.512195 ± 4	18.5533 ± 4	15.6259 ± 4	39.0275 ± 12	88.7	25.9	13.0
32	Inabe	65	0.723109 ± 5	0.512168 ± 5	18.5620 ± 4	15.6457 ± 4	38.9673 ± 10	76.0	20.8	23.0
		66	0.722643 ± 4	0.512170 ± 5	18.5998 ± 4	15.6466 ± 4	38.9766 ± 12	77.5	20.2	18.0
33	Ibi	67	0.723710 ± 5	0.512084 ± 4	18.7478 ± 5	15.6498 ± 5	39.0019 ± 15	74.9	19.6	10.7
		68	0.727368 ± 5	0.512033 ± 6	18.7796 ± 6	15.6590 ± 5	39.0770 ± 15	69.4	21.4	9.9
34	Nagara	69	0.720115 ± 5	0.512162 ± 7	18.5836 ± 4	15.6419 ± 4	38.9230 ± 11	100.1	19.2	11.1
		70	0.720535 ± 5	0.512065 ± 5	18.6192 ± 3	15.6455 ± 3	38.9797 ± 9	110.1	24.7	13.8
35	Kiso	71	0.711262 ± 5	0.512222 ± 7	18.4788 ± 4	15.6302 ± 4	38.8459 ± 11	177.7	19.4	19.1
		72	0.712987 ± 4	0.512055 ± 4	18.4953 ± 5	15.6333 ± 5	38.8766 ± 14	136.6	19.6	18.6
36	Shonai	73	0.721051 ± 4	0.512098 ± 5	18.5135 ± 4	15.6350 ± 4	38.7215 ± 11	54.6	21.3	22.3
		74	0.720296 ± 5	0.512099 ± 4	18.4899 ± 4	15.6308 ± 4	38.6969 ± 12	56.0	20.7	22.3

(*continued on next page*)

Table 1 (*continued*)

River no.	River name	Sample no.	$^{87}Sr/^{86}Sr$	$^{143}Nd/^{144}Nd$	$^{*206}Pb/^{204}Pb$	$^{*207}Pb/^{204}Pb$	$^{*208}Pb/^{204}Pb$	Sr (mg/kg)	Nd (mg/kg)	Pb (mg/kg)
37	Yahagi	75	0.715066 ± 6	0.512199 ± 5	18.4821 ± 2	15.6301 ± 2	38.7627 ± 6	50.3	13.5	11.7
		76	0.715025 ± 6	0.512189 ± 6	18.4608 ± 2	15.6288 ± 2	38.7371 ± 7	53.0	13.5	12.2
		77	0.714624 ± 6	0.512186 ± 12	18.3846 ± 2	15.6222 ± 2	38.6137 ± 5	39.3	7.3	10.0
38	Toyo	78	0.712097 ± 5	0.512338 ± 4	18.4680 ± 4	15.6216 ± 4	38.6331 ± 11	71.8	13.1	10.0
39	Tenryu	79	0.712181 ± 4	0.512308 ± 5	18.5933 ± 5	15.6267 ± 5	38.8732 ± 15	129.3	20.7	8.4
		80	0.712374 ± 4	0.512344 ± 7	18.6202 ± 5	15.6180 ± 4	38.8693 ± 11	106.2	26.5	9.4
40	Oi	81	0.712382 ± 5	0.512369 ± 4	18.6235 ± 4	15.6122 ± 4	38.8715 ± 13	102.1	27.9	8.3
		82	0.713141 ± 4	0.512377 ± 4	18.6416 ± 5	15.6141 ± 5	38.8832 ± 15	77.7	16.7	6.5
		83	0.712955 ± 4	0.512360 ± 4	18.6381 ± 4	15.6125 ± 4	38.8836 ± 10	96.6	24.4	6.6
41	Abe	84	0.712576 ± 4	0.512323 ± 8	18.5228 ± 5	15.6057 ± 5	38.7639 ± 14	89.0	23.5	7.9
		85	0.711154 ± 5	0.512317 ± 8	18.5183 ± 6	15.6056 ± 5	38.7773 ± 14	117.3	20.7	5.7
42	Fuji	86	0.708856 ± 5	0.512403 ± 8	18.4763 ± 4	15.5972 ± 4	38.6671 ± 10	133.4	16.8	8.9
		87	0.709105 ± 4	0.512371 ± 4	18.5155 ± 5	15.6048 ± 5	38.7341 ± 13	197.2	24.6	7.5
		88	0.709339 ± 5	0.512353 ± 5	18.5142 ± 4	15.6047 ± 4	38.7227 ± 13	116.4	17.6	5.4
43	Kano	89	0.705099 ± 4	0.512761 ± 7	18.2719 ± 5	15.5592 ± 4	38.2578 ± 12	84.6	6.1	7.5
		90	0.704669 ± 4	0.512811 ± 7	18.2806 ± 4	15.5526 ± 4	38.2610 ± 12	94.1	5.4	6.8
		91	0.704854 ± 4	0.512751 ± 12	18.2114 ± 4	15.5656 ± 4	38.1951 ± 10	97.6	5.9	8.4
44	Sakawa	92	0.703975 ± 5	0.512940 ± 9	18.1605 ± 4	15.5541 ± 4	38.1309 ± 10	196.8	5.3	4.6
45	Sagami	93	0.705849 ± 4	0.512490 ± 5	18.2927 ± 5	15.5843 ± 4	38.3592 ± 12	151.1	11.8	9.9
		94	0.705843 ± 5	0.512528 ± 11	18.2353 ± 4	15.5866 ± 4	38.2948 ± 11	52.6	4.1	5.4
		95	0.706644 ± 5	0.512515 ± 7	18.3005 ± 5	15.5832 ± 5	38.3774 ± 12	78.9	7.2	6.7
46	Tama	96	0.712013 ± 5	0.512331 ± 8	18.4805 ± 4	15.6181 ± 4	38.6091 ± 12	86.4	11.3	9.0
		97	0.711905 ± 5	0.512319 ± 6	18.5171 ± 5	15.6206 ± 5	38.6540 ± 14	112.4	14.5	11.3
47	Ara	98	0.711170 ± 6	0.512371 ± 6	18.4854 ± 2	15.6111 ± 2	38.6192 ± 6	75.7	11.7	8.3
		99	0.711365 ± 6	0.512336 ± 6	18.4516 ± 2	15.6122 ± 2	38.5830 ± 6	72.0	12.1	10.3
		100	0.710964 ± 7	0.512369 ± 5	18.4424 ± 2	15.6115 ± 2	38.5722 ± 6	76.5	11.1	9.7
48	Tone	101	0.708446 ± 6	0.512419 ± 5	18.3791 ± 2	15.5955 ± 2	38.5149 ± 5	94.2	10.9	10.9
		102	0.708533 ± 5	0.512415 ± 5	18.3798 ± 2	15.5984 ± 2	38.5216 ± 6	89.2	10.8	10.8

* Repeated analyses of an in-house standard sample, Cica-Pb, at KCC obtained average $^{206}Pb/^{204}Pb$ of 18.077 ± 1 (2σ) (n = 21), $^{207}Pb/^{204}Pb$ of 15.599 ± 1 (2σ) (n = 21), and $^{208}Pb/^{204}Pb$ of 38.006 ± 4 (2σ) (n = 21). These values correspond to $^{206}Pb/^{204}Pb$ of 16.931, $^{207}Pb/^{204}Pb$ of 15.484, and $^{208}Pb/^{204}Pb$ of 36.676 in NIST SRM 981. Repeated analyses of a NMIJ CRM 3681-a, which is a standard sample provided by AIST, Japan, at RIHN obtained average values of $^{206}Pb/^{204}Pb$ of 18.053 ± 1 (2σ) (n = 16), $^{207}Pb/^{204}Pb$ of 15.589 ± 1 (2σ) (n = 16), and $^{208}Pb/^{204}Pb$ of 37.955 ± 4 (2σ) (n = 16). These values correspond to $^{206}Pb/^{204}Pb$ of 16.921, $^{207}Pb/^{204}Pb$ of 15.469, and $^{208}Pb/^{204}Pb$ of 36.627 in NIST SRM 981.

$^{208}Pb/^{204}Pb$ = 38.2–38.7), represent one isotopic compositional extreme. These characteristics are particularly pronounced in the sediment samples from the Kano and Sakawa rivers (nos. 43 and 44) with watersheds in the Izu-Honshu collision zone. Similarly, the isotopic compositions of Ce-V sediments are characterized by high $^{143}Nd/^{144}Nd$ and low $^{87}Sr/^{86}Sr$, $^{206}Pb/^{204}Pb$, $^{207}Pb/^{204}Pb$, and $^{208}Pb/^{204}Pb$ values.

The other compositional extreme is represented by J-A-i sediments, which have high $^{87}Sr/^{86}Sr$ (0.720–0.728), low $^{143}Nd/^{144}Nd$ (0.5120–0.5122), and generally high Pb isotope ratios ($^{206}Pb/^{204}Pb$ = 18.4–18.8; $^{207}Pb/^{204}Pb$ = 15.62–15.66; $^{208}Pb/^{204}Pb$ = 38.6–39.1). Remarkably, the isotopic characteristics of J-A-o sediments are quite different from those of J-A-i sediments; $^{87}Sr/^{86}Sr$ and $^{143}Nd/^{144}Nd$ ratios of J-A-o sediments are intermediate between those of Q-V and J-A-i sediments. In addition, $^{208}Pb/^{207}Pb$ is distinctively low in relation to $^{206}Pb/^{207}Pb$, compared with those of J-A-i sediments. Cr-M sediments are isotopically similar to J-A-o sediments.

The $^{87}Sr/^{86}Sr$ and Pb isotope ratios of Cr-A sediments and Cr-P sediments are similar, but $^{143}Nd/^{144}Nd$ ratios of Cr-P sediments are slightly lower than those of Cr-A sediments.

5. Discussion

5.1. Regional variation in relation to watershed geology

The Sr-Nd-Pb isotope ratios of river sediments are concordant with the formative history of the main geological unit in each watershed.

Because magmas around subduction zones are usually derived from melting of mantle metasomatized by fluid in the subducted slab (Tatsumi, 1989), $^{87}Sr/^{86}Sr$ and $^{143}Nd/^{144}Nd$ values of young arc volcanic rocks tend to be relatively low and high, respectively (Fig. 3). Therefore, it is reasonable that the sediments derived from Quaternary volcanic rocks should have relatively low $^{87}Sr/^{86}Sr$ and high $^{143}Nd/^{144}Nd$. Sr and Nd isotopic compositions of Q-V sediments from the Kano and Sakawa rivers (river nos. 43 and 44) are probably largely controlled by the low $^{87}Sr/^{86}Sr$ and high $^{143}Nd/^{144}Nd$ values of the volcanic rocks distributed in their watersheds, which are located in the Izu-Honshu collision zone (Mt. Fuji, $^{87}Sr/^{86}Sr$ = 0.7033–0.7035, $^{143}Nd/^{144}Nd$ = 0.5130–0.5131, Nagai et al., 2004; Izu Bonin arc, $^{87}Sr/^{86}Sr$ = 0.7030–0.7038, $^{143}Nd/^{144}Nd$ = 0.5130–0.5131, Tailor and Nesbitt, 1998). Volcanic rocks on Kyushu Island exhibit slightly higher $^{87}Sr/^{86}Sr$ and lower $^{143}Nd/^{144}Nd$ values (Sakurajima Island, $^{87}Sr/^{86}Sr$ = 0.7042–0.7057, $^{143}Nd/^{144}Nd$ = 0.5125–0.5128, Shibata et al., 2013; Mt. Aso, $^{87}Sr/^{86}Sr$ = 0.7040–0.7042, $^{143}Nd/^{144}Nd$ = 0.5127–0.5128, Hunter, 1998), and these values are consistent with the isotope compositions of Q-V sediments in the Kyushu area (river nos. 2, 10, 11, and 12).

The isotopic dissimilarity between J-A-i sediments and J-A-o sediments (Fig. 3) may reflect the isotopic characteristics of the J-A-i and J-A-o source rocks, which may have been separated by up to a thousand kilometers before becoming juxtaposed during the Cretaceous Period as a result of left-lateral strike-slip motion along the MTL (e.g., Sakashima et al., 2003). Sr-Nd isotope ratios of the J-A-o and Cr-A sediments exhibit good consistency with those of the Cretaceous to Paleogene sandstones and mudstones of the Shimanto Belt in the Outer Zone ($^{87}Sr/^{86}Sr$ = 0.711–0.716, $^{143}Nd/^{144}Nd$ = 0.5122–0.5124, Terakado et al., 1988). Unfortunately, information on the Sr and Nd isotope ratios in sedimentary rocks of the Inner Zone is not available.

Cr-M sediments are isotopically similar to J-A-o and Cr-A sediments (Fig. 3). This can be related to that the rocks of Cr-M are mainly metamorphosed from rocks of J-A-o and Cr-A (Isozaki and Itaya, 1990; Nakajima, 1994; Okamoto et al., 2000). Cr-M is dominant in the watersheds of the Yoshino (river no. 19), Kushida (river no. 29), and Toyo (river no. 38) rivers. In the Yoshino and Kushida river watersheds, in particular, the areal proportion of Cr-M, which in these watersheds consists of Sanbagawa Belt rocks, exceeds 50%. The rocks of the Sanbagawa Belt, which were metamorphosed under high pressure/low

temperature condition (Miyashiro, 1961), are composed of basic, pelitic, and quartz schists. The Sr-Nd isotope ratios of Cr-M sediments are similar to those of pelitic schists but quite different from those of basic schist (Uno et al., 2014) (Fig. 3). This result suggests that the pelitic schists are the main source of the Cr-M sediments. The Pb isotope ratios of the Cr-M sediments also indicate that the main source rock of the Cr-M sediments is the pelitic schist. Although these ratios of Cr-M sediments are higher than those of pelitic schists, they are well aligned along the line passing through the compositional area of the pelitic schists in plots among $^{206}Pb/^{204}Pb$, $^{207}Pb/^{204}Pb$, and $^{208}Pb/^{204}Pb$. This can be explained by the excess of extremely radiogenic zircons, monazites and allanites in sediments over in the source rocks due to their resistibility for chemical weathering and their very high U/Pb and Th/Pb ratios (Garcon et al., 2013).

Cr-P sediments have isotopic ratios intermediate between those of J-A-i and sediments from volcanic watersheds (Q-V and Ce-V), with the exception of the Kumode River (no. 30) sediments (Fig. 3). Sr-Nd isotope ratios of Cr-P sediments differ from those of the granitic rocks of the Ryoke Belt (Kagami et al., 1992; Okano et al., 2000); their $^{87}Sr/^{86}Sr$ ratios are higher and $^{143}Nd/^{144}Nd$ ratios are lower than the corresponding values of the source rocks (Fig. 3). These differences may be due to differential weathering; fine sediments produced by weathering of granitic rocks are derived primarily from biotite and feldspar (e.g., Aubert et al., 2001; Blum and Erel, 1997). Thus, clay minerals produced by the weathering of these minerals may dominantly account for the isotopic composition of the Cr-P sediments. In fact, biotite from Ryoke granitic rocks has an extremely high $^{87}Sr/^{86}Sr$ ratio (~0.86), and feldspar from these rocks has relatively low $^{143}Nd/^{144}Nd$ ratios (0.51230–0.51235; Okano et al., 2000).

The ranges of the Sr and Nd isotope ratios of Ce-A sediments are as large as those of the aggregated sediments from the other accretionary-prism watersheds (J-A-i, J-A-o, and Cr-A) although the ranges of the Pb isotope ratios of Ce-A sediments are rather narrow ($^{206}Pb/^{204}Pb$ = 18.47–18.55; $^{207}Pb/^{204}Pb$ = 15.60–15.63; $^{208}Pb/^{204}Pb$ = 38.76–38.84) (Fig. 3). The $^{87}Sr/^{86}Sr$ ratio of Ce-A sediments tends to decrease eastward, whereas the $^{143}Nd/^{144}Nd$ ratio increases eastward (Fig. 4). Given that isotopic values of Ce-A sediments straightforwardly reflect those of their source sedimentary rocks, this wide isotopic variation is inferred to indicate differences in the provenance of the source rocks. In particular, these results suggest that during the Eocene to early Miocene, volcanic rocks were distributed mainly on the eastern side of the southwest Japan arc.

5.2. Isotopic dissimilarity among sediments derived from the main geological units

The wide variation of the isotope ratios of fine sediments due to differences in watershed geology is expected to be useful for interpreting the origin of hemipelagic sediments around Japan. However, although isotope ratios of river sediments are apparently explained by the principal geological units in each watershed as described above, it should be noted that the subordinate units can be a major contributor of sediments due to the high vulnerability of their rocks to weathering and erosion. In order to examine the possibility of high contribution from the subordinate units, we compared the isotope ratios of sediments derived from the five geological units with the widest distribution among the studied watersheds (J-A, Cr-A, Q-V, Cr-P, and Cr-M) with the areal ratio of surface exposure of those units in each watershed and found that the isotopic ratios of the sediments, except those of J-A sediments, tended to converge on certain values as the areal ratio of the geological unit increased (Fig. 5). When J-A watersheds in the Inner and Outer zones were considered separately, however, the isotopic ratios of the J-A sediments also converged. This result suggests that, at least for these 6 geological units (J-A-i, J-A-o, Cr-A, Q-V, Cr-P, and Cr-M), when each of them exceeds the half of the watershed in area, sediments with relatively homogeneous isotopic ratios particular to each unit are yielded reflecting the principal geological unit.

If the isotope ratios of sediments from watersheds where J-A-i, J-A-o, Cr-A, Q-V, Cr-P, or Cr-M occupy more than half of the watershed area are considered to be representative of each geological unit, then these units can be discriminated by considering the Sr-Nd-Pb isotope ratios in combination. The representative isotope ratios of J-A-i, J-A-o, Cr-A, Q-V, Cr-P, and Cr-M sediments are compared in Fig. 6. J-A-i sediments and Q-V sediments can be easily discriminated from the other geological units on the basis of their $^{87}Sr/^{86}Sr$ ratios (very high in J-A-i sediments and very low in Q-V sediments). The $^{143}Nd/^{144}Nd$ ratios also differ considerably among J-A-o, Cr-A, and Cr-P sediments. Cr-M sediments are distinguishable from other sediments by their relatively high $^{206}Pb/^{204}Pb$ ratios, and they can be more clearly distinguished from Cr-A sediments by considering their $^{143}Nd/^{144}Nd$ and $^{206}Pb/^{204}Pb$ ratios in combination, and from J-A-o sediments by considering their $^{206}Pb/^{204}Pb$ and $^{208}Pb/^{204}Pb$ values in combination.

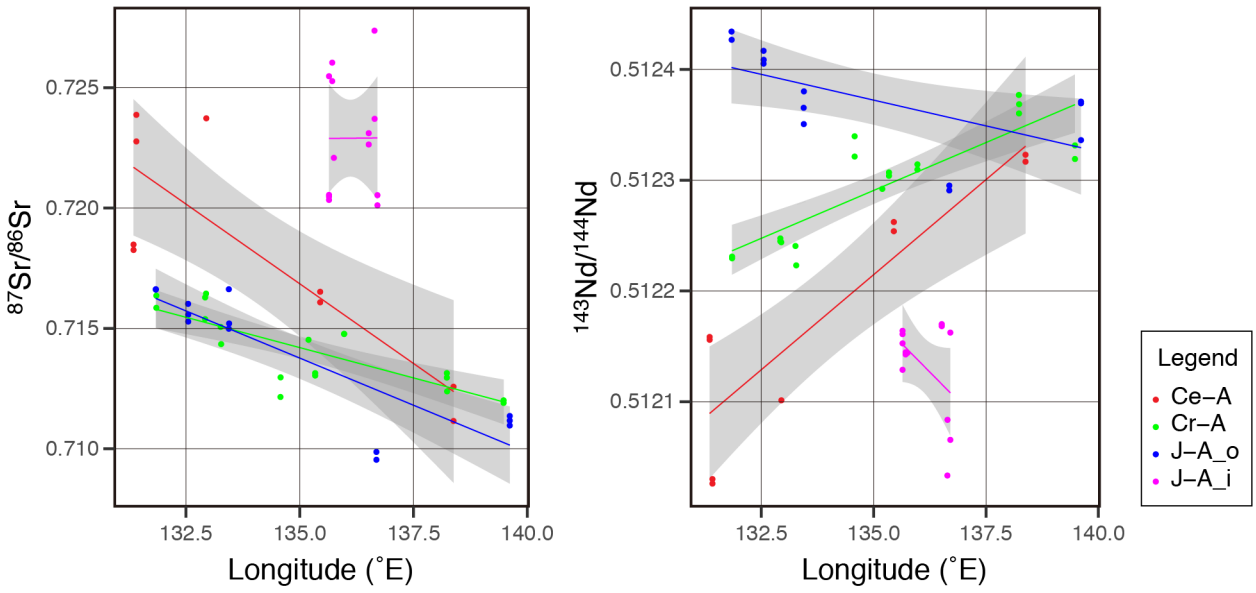

Fig. 4. Longitudinal changes in Sr–Nd isotope ratios of J-A-i, J-A-o, Cr-A, and Ce-A sediments. Gray shading indicates the 95% confidence intervals in the linear regression results.

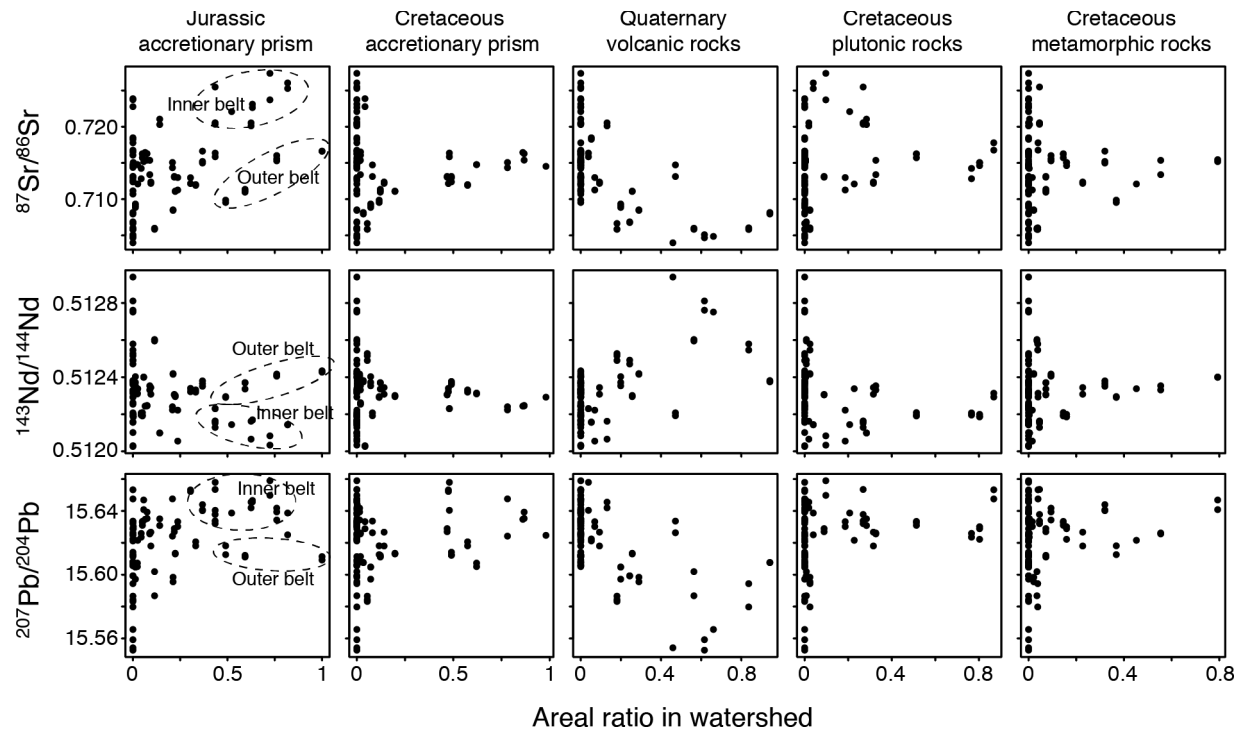

Fig. 5. Relationships between isotope ratios in each watershed and the areal ratio of surface exposure of each geological unit in the same watershed.

The principal component analysis (PCA) of these representative isotope ratios can show the degree of discrimination among the units more quantitatively. PCA was conducted using R (R Core Team, 2019) for the standardized values of the 5 isotope ratios ($^{87}Sr/^{86}Sr$, $^{143}Nd/^{144}Nd$, $^{206}Pb/^{204}Pb$, $^{207}Pb/^{204}Pb$, and $^{208}Pb/^{204}Pb$) as the variables. The resultant first three principal components PC1, 2, and 3 can explain 98% of the variables (Table A.2). Plots of the scores of these 3 PCs with 90-% normal confidence ellipses show that the J-A-i, Cr-P, Cr-M, and Q-V sediments can be discriminated from one another with high (at least 81%) probability (Fig. 7). In the same level of probability, J-A-o sediments can be differentiated from Cr-P and J-A-i sediments, and Cr-A sediments can be from Q-V and J-A-i sediments. Q-V can be differentiated from all but J-A-o sediments. On the other hand, examination of individual isotope ratio is also shown to be important considering that $^{143}Nd/^{144}Nd$ ratios of the J-A-o and Cr-A sediments, which cannot be distinguished by PCA, are clearly different from one another (Fig. 6).

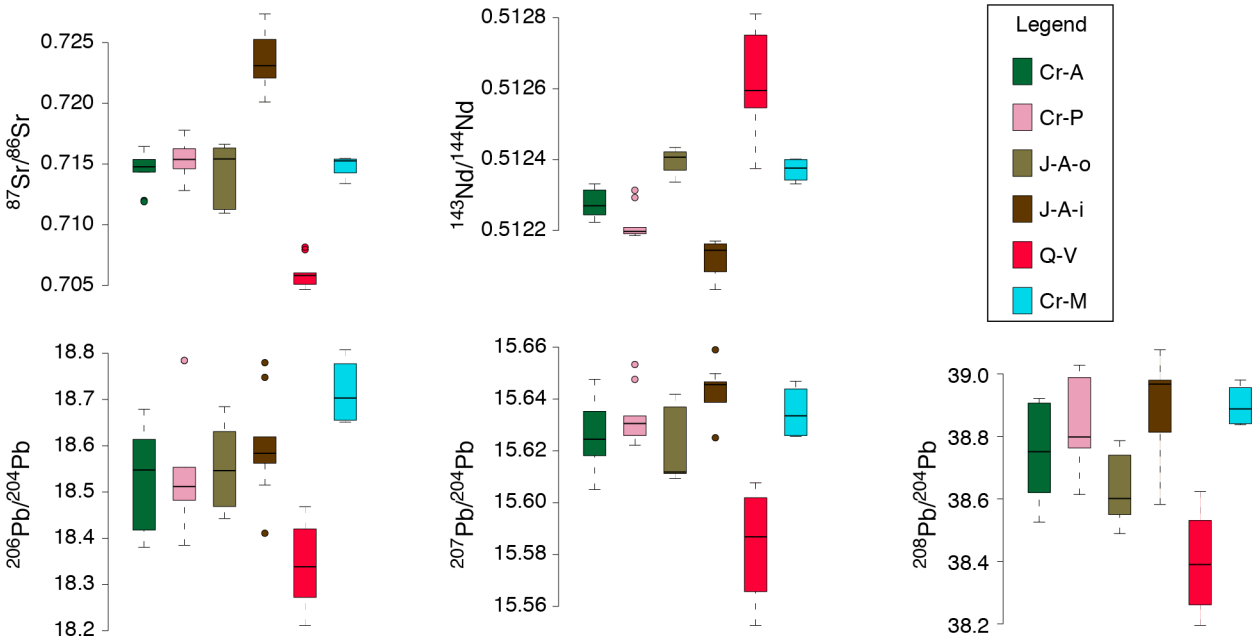

Fig. 6. Box plots of isotope ratios of the six main geological units. The bar across the box means median value. The lower and upper ends of the box represent the lower and upper quatile points (X0.25 and X0.75), respectively. The lower whisker indicates the larger value of X0.25 - (X0.75 − X0.25) × 1.5 and the minimum data. The upper whisker does the smaller value of X0.75 + (X0.75-X0.25) × 1.5 and the maximum data. Plots outside of the upper and lower whiskers are considered as outliers.

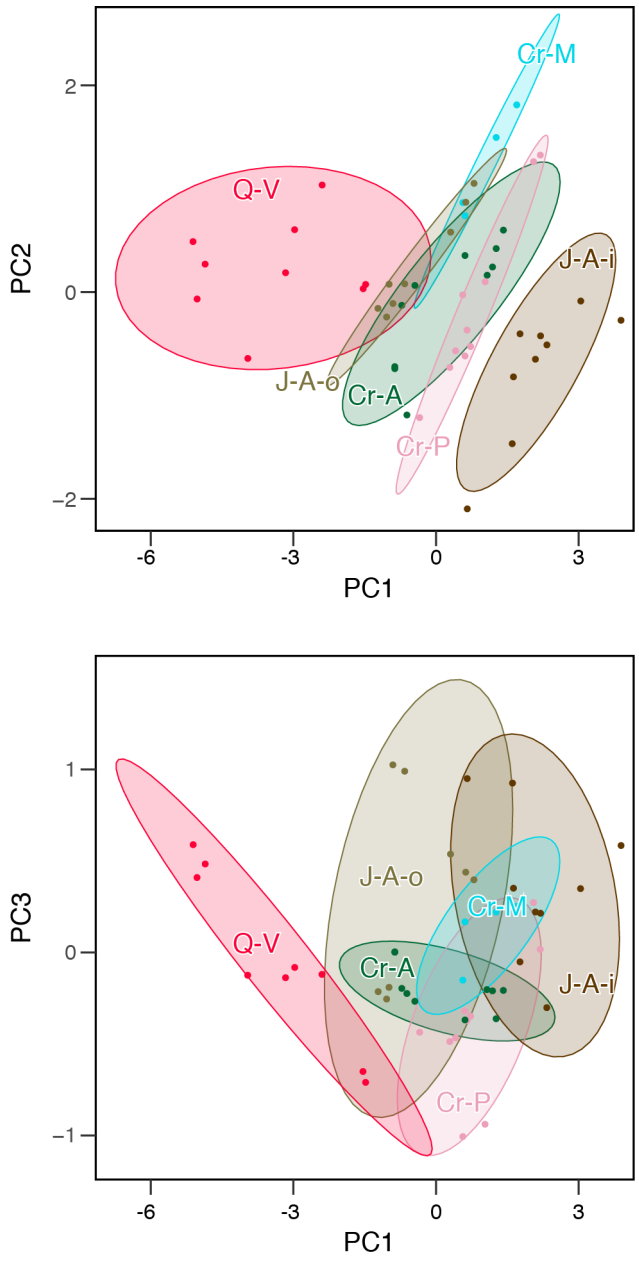

Fig. 7. Plots of the first three principal component scores derived from the isotope ratios of sediments from watersheds where J-A-i, J-A-o, Cr-A, Q-V, Cr-P, or Cr-M occupy more than half of the watershed area. Ellipses indicate the probability of 90%.

5.3. Sediments in the North Pacific Ocean and possible sources

To examine possible long-distance transport of sediments by the KC, we compared Sr-Nd-Pb isotopic compositions of deep-sea core sediments from four coring sites in the North Pacific with several possible sources of mineral particles (Figs. 8 and 9). At present, Integrated Ocean Drilling Program (IODP) site C0011 in the Shikoku Basin is strongly influenced by the KC. ODP site 1208, on the Shatsky rise, is located along the flow path of the Kuroshio Extension, although it is about 1700 km to the east of the Japanese archipelago. In contrast, ODP site 885/886 and site L44-GPC3 are located further east, in the high and middle latitudes of the central Pacific, respectively, where they are unlikely to be influenced by the KC. Here, we consider data from C0011 covering the period from 7 Ma to the present (Saitoh et al., 2015), and data from ODP 1208 (Zhang et al., 2016), ODP 885/886 (Pettke et al., 2000), and L44-GPC3 (Pettke et al., 2002) covering the Plio-Pleistocene interval (from ~5 Ma to the present). Although earlier data are available for the latter 3 sites, we have restricted the period under consideration so that modern oceanographic and atmospheric conditions can be assumed.

Asian dust, which is derived from arid areas of inland China, is a major component of detrital particles deposited in pelagic areas of the north Pacific (e.g., Asahara et al., 1995; Ferguson et al., 1970; Jones et al., 1994; Nakai et al., 1993; Rea et al., 1985; Uematsu et al., 1983; Windom, 1969). In particular, the desert areas along the northern margin of the Tibetan Plateau and on the Ordos Plateau have been the main contributors to dust deposition in the North Pacific and in Greenland (Chen et al., 2007). Here, Sr-Nd isotope ratios of fine particles (< 5 μm) from these deserts (Chen et al., 2007) and Sr-Nd-Pb isotope ratios of Chinese loess from the Loess Plateau (Sun, 2005; Sun and Zhu, 2010), the most proximal deposits of Asian dust, are used as Asian dust indicators.

Volcanic ashes are another important component of the aeolian flux to the North Pacific (Nakai et al., 1993; Olivarez et al., 1991). Volcanoes of the Japanese archipelago, Kuril Islands, and Kamchatka Peninsula are possible sources of volcanic ashes to the North Pacific. Here, Sr-Nd-Pb isotope ratios of Miocene to Holocene volcanic rocks from these areas in the GEOROC database (http://georoc.mpch-mainz.gwdg.de/georoc/) are used as indicators of volcanic ashes.

Considering its flow path (Fig. 1A), the KC is expected to entrain sediments discharged from Taiwan, the Chinese mainland, and southwest Japan before it turns eastward and flows away from Japan as the Kuroshio Extension. Here, Sr-Nd-Pb isotope ratios of river sediments of southwest Japan (this study), Taiwan (Zheng et al., 2016), the lower courses of the Changjiang (Yangtze River; Meng et al., 2008; Yang et al., 2007) and Huanghe (Yellow River; Meng et al., 2008), seafloor sediments around the ECS (Bentahila et al., 2008; Dou et al., 2012; Saitoh et al., 2015), and Pliocene hemipelagic mudstones in the Ryukyu Islands (Saitoh et al., 2015) are compared with those of the deep-sea core sediments.

5.3.1. North central Pacific sediments

Sr-Nd-Pb isotope ratios of sediments from sites L44-GPC3 and ODP 885/886 are reasonably explained by the mixing of Asian dust and volcanic ashes (Pettke et al., 2000; Pettke et al., 2002). The possibility that any sediments are supplied to these distant sites from land areas along the KC path is excluded by their Pb isotope ratios. The $^{206}Pb/^{204}Pb$ ratios, in relation to $^{208}Pb/^{204}Pb$, of sediments in the possible source areas of Kuroshio transport, southwest Japan and sediments around the ECS, are clearly lower than those of Chinese loess (Fig. 9). In addition, the Pb isotope ratios of the L44-GPC3 and ODP 885/886 sediments clearly support the previous inference (Pettke et al., 2000; Pettke et al., 2002) that the volcanic sources of ashes in sediments at these sites were in Kamchatka rather than in Japan or the Kuril Islands. The $^{208}Pb/^{204}Pb$ versus $^{206}Pb/^{204}Pb$ plots of the sediments from these sites lie along the mixing line between Chinese loesses and volcanic rocks in Kamchatka. Thus, at these distant sites, particle transport by the Kuroshio Extension can be excluded.

5.3.2. Shikoku Basin sediments

On the basis of sediment Sr-Nd-Pb isotope ratios, Saitoh et al. (2015) interpreted the sediments of IODP site C0011 in the Shikoku Basin to consist of material derived from southwest Japan and transported by the KC from around the ECS. The $^{206}Pb/^{204}Pb$ and $^{208}Pb/^{204}Pb$ relations in C0011 sediments are consistent with those in ECS and Japanese river sediments, but not with those in Chinese loess, thus excluding the possibility of a substantial contribution of Asian dust. However, because Saitoh et al. (2015) did not comprehensively consider the Sr-Nd-Pb isotope ratios of all possible Japanese sediment sources, there has remained the possibility that the C0011sediments are all supplied from southwest Japan.

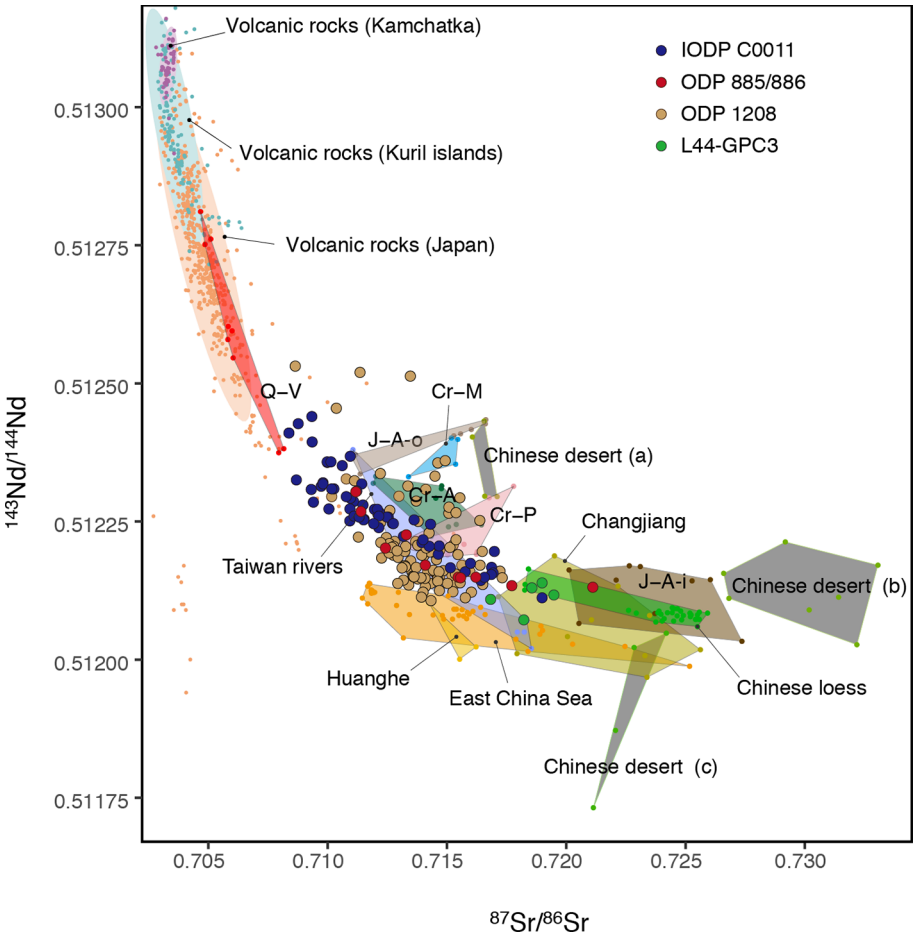

Fig. 8. Comparison of Sr–Nd isotope ratios of deep-sea sediments in the North Pacific (L44-GPC3; Pettke et al., 2000; ODP 885/886: Pettke et al., 2002; ODP1208: Zhang et al., 2016; IODP C0011: Saitoh et al., 2015) with those of sediments in possible sources, Chinese loess (Sun, 2005), Chinese desert (Chen et al., 2007), Volcanic rocks along the western margin of the North Pacific (GEOROC, http://georoc.mpch-mainz.gwdg.de/georoc/), Taiwanese rivers (Zheng et al. 2016), Changjiang (Yang et al., 2007; Meng et al., 2008), East China Sea (Dou et al., 2012; Saitoh et al., 2015), and rivers in southwest Japan dominated by the 6 major geological units (J-A-i; Jurassic accretionary complex in the inner belt, J-A-o; Jurassic accretionary complex in the Outer Zone, Cr-A; Cretaceous accretionary complex, Cr-M; Cretaceous metamorphic rocks, Cr-P; Cretaceous plutonic rocks, and Q-V; Quaternary volcanic rocks).

Comparison of the isotope composition of the C0011 sediments with those of the river sediments determined in this study shows that only Q-V and J-A-i sediments could have contributed to the sediments deposited at site C0011. The Sr-Nd isotope ratios of J-A-o and Cr-M sediments plot away from those of the C0011 sediments. Q-V sediments from around the Izu-Honshu collision zone are known to be delivered by turbidity flows directly to the Nankai Trough via undersea canyons (e.g., Taira and Niitsuma, 1986), and fine particles in such turbidity flows might spill over from the trough into the outer Shikoku Basin (Pickering et al., 1992). Nepheloid-layer transport from the Izu-Bonin ridge might also contribute to Shikoku Basin sediments (Underwood and Fergusson, 2005). Contribution of Cr-A and Cr-P sediments should have been scarce considering that their overlaps with C0011 sediments are very small in plots of Sr-Nd isotope ratios. Although Sr-Nd-Pb isotopic compositions of J-A-i sediments are consistent with those of C0011 sediments, it is unlikely that J-A-i, which is distributed more distantly from the Pacific coast of southwest Japan than Cr-A, J-A-o, Cr-P, and Cr-M, had discharged large amounts of sediments into the Pacific during Plio-Pleistocene time. In southwest Japan, gravels derived from Cr-P and Cr-M commonly occur in Miocene strata (e.g., Kusuhashi and Yamaji, 2001; Shibata, 1967; Yoshida, 1987); therefore, the Outer Zone, which includes these geological units, were already widely exposed in southwest Japan when the C0011 sediments were deposited (< 7 Ma). Thus, if J-A-i had supplied large amounts of sediments to the Pacific during this interval, then the J-A-o, Cr-A, Cr-P and Cr-M terranes of the Outer Zone, which are located closer to the Pacific, should have supplied amounts of sediments comparable to those supplied by J-A-i, and the influence of J-A-o, Cr-A, Cr-P and Cr-M should also be seen in the Sr-Nd isotope ratios of the C0011 sediments. These considerations suggest that Q-V sediments from southwest Japan and sediments from land areas around the ECS are the main sources of the C0011 sediments. The Sr-Nd isotope ratios of river sediments from Taiwan are consistent with those of the C0011 sediments, so Taiwan, in addition to other areas around the ECS, might be a source of sediments in the Shikoku Basin.

5.3.3. *Shatsky rise sediments*

The Sr-Nd isotope ratios of sediments from ODP Site 1208 on the Shatsky rise are rather scattered compared with those of sediments in the north central Pacific and the Shikoku Basin (Fig. 8). Some values overlap the isotopic ranges of river sediments from southwest Japan and Taiwan. Because the Shatsky rise is located along the Kuroshio Extension flow path, it is likely that fine particles are transported by the KC from southwest Japan and the ECS region. Indeed, the importance of ocean-current transport is suggested by the occurrence of pollen and spores derived from southern Japan and the area around the ECS in sediments on the Hess rise (Kawahata and Ohshima, 2002), which is also located further along the Kuroshio Extension flow path than the Shatsky rise. Although Zhang et al. (2016) argued that the scatter of Sr-Nd isotope ratios is due to the heterogeneities of volcanic ash and Asian dust, the possibility that particles transported by the KC contributed to detrital deposition on the Shatsky rise cannot be excluded. Measurement of Pb isotope ratios of the sediments from ODP Site 1208 is required to constrain the possible sources of sediments at the site.

6. Conclusions

The Sr-Nd-Pb isotope ratios of the fine fraction (< 20 μm) of river sediments in southwest Japan, which vary widely depending on the dominant geological unit exposed in the watersheds of the rivers, are

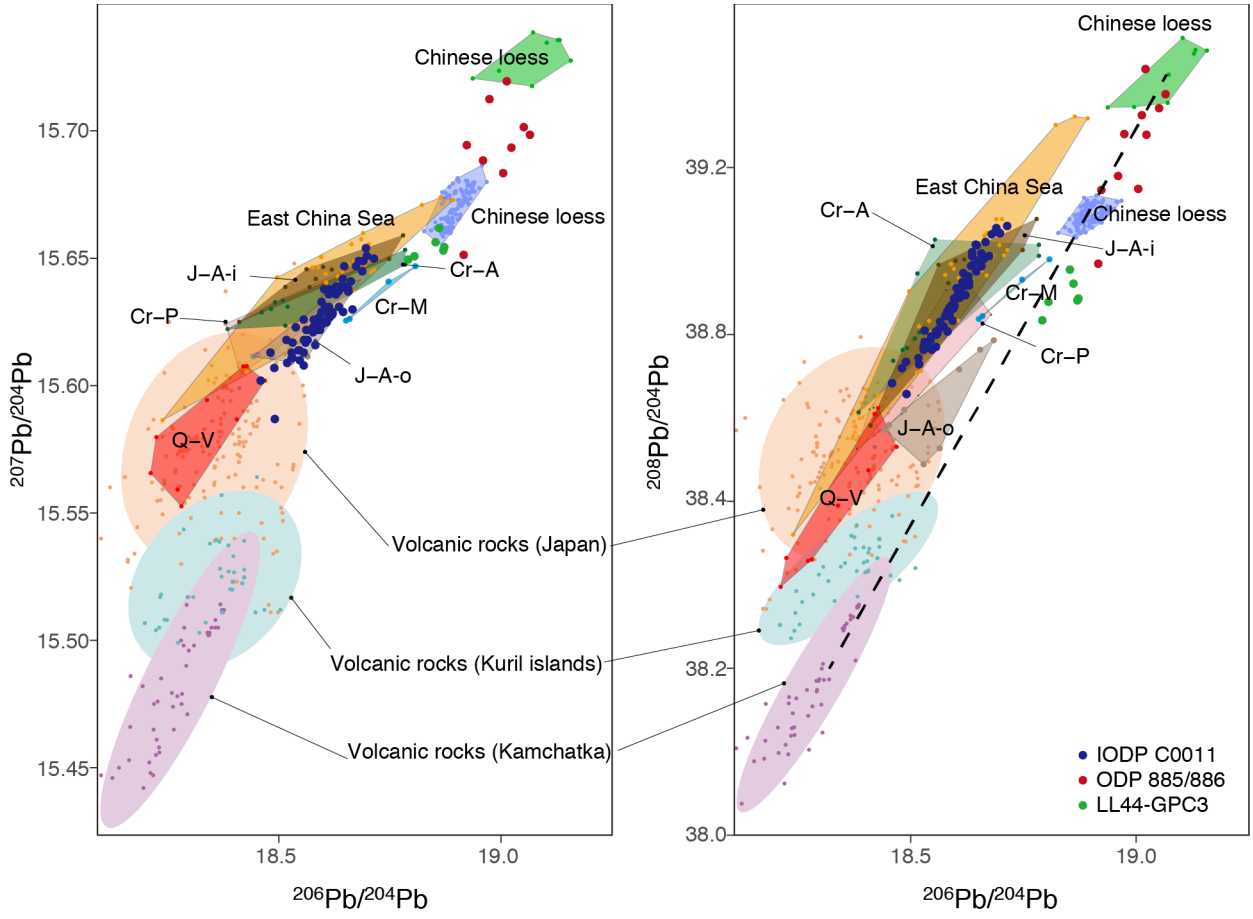

Fig. 9. Comparison of Pb isotope ratios of deep-sea sediments in the North Pacific (L44-GPC3; Pettke et al., 2000; ODP 885/886: Pettke et al., 2002; ODP1208: Zhang et al., 2016; IODP C0011: Saitoh et al., 2015) with those of sediments in the possible sources, Chinese loess (Sun and Zhu, 2010, green; Jones et al., 2000, violet), volcanic rocks along the western margin of the North Pacific (GEOROC, http://georoc.mpch-mainz.gwdg.de/georoc/), East China Sea (Bentahila et al., 2008,; Saitoh et al., 2015), and rivers in southwest Japan dominated by the 6 major geological units (J-A-i; Jurassic accretionary complex in the inner belt, J-A-o; Jurassic accretionary complex in the Outer Zone, Cr-A; Cretaceous accretionary complex, Cr-M; Cretaceous metamorphic rocks, Cr-P; Cretaceous plutonic rocks, and Q-V; Quaternary volcanic rocks). Isotope ratios of LL44-GPC3, ODP 885/886, IODP C0011 and East China Sea sediments have been corrected against NIST SRM 981 values ($^{206}Pb/^{204}Pb$ = 16.9308; $^{207}Pb/^{204}Pb$ = 15.4839; $^{208}Pb/^{204}Pb$ = 36.6743; Tanimizu and Ishikawa, 2006).

presented. The isotope ratios can be well explained by the lithology, origin, and formative history of each geological unit. When used in combination, Sr-Nd-Pb isotope ratios of these fine sediments can be used to clearly discriminate the major geological units distributed in the watersheds. Therefore, the Sr-Nd-Pb isotope ratios of fine sediments are sensitive indicators of the source geology and can be effectively used to estimate sources of hemipelagic sediments occurring on the seafloor of the northwest Pacific.

Importance of the KC in long-distance transport of fine particles in the Northwest Pacific is suggested. Comparison of the isotopic data of southwest Japan river sediments analyzed in this study with those of sediments in the north Pacific corroborates the previous interpretation (Pettke et al., 2000; Pettke et al., 2002) that the sediments from the sites ODP 885/886 and LL4-GPC3, which are located in the central North Pacific, are composed of a simple mixture of Asian dust and volcanic ash. In contrast, sediments from site IODP C0011, which is located at the north end of the Shikoku Basin, are interpreted in this study to be composed of sediments derived from Quaternary volcanic rocks in southwest Japan, and also of sediments from land areas around the ECS by the KC as suggested by Saitoh et al. (2015). The KC may also have transported detrital particles from southwest Japan to site ODP 1208 on the Shatsky rise, considering the Sr-Nd isotope ratios of sediments at that site, although measurement of Pb isotope ratios is needed to confirm this possibility.

CRediT authorship contribution statement

Yu Saitoh: Conceptualization, Investigation, Writing - original draft, Writing - review & editing. **Masaharu Tanimizu:** Methodology, Writing - original draft. **Tsuyoshi Ishikawa:** Methodology, Writing - original draft.

Declaration of Competing Interest

The authors declare that they have no known competing financial interests or personal relationships that could have appeared to influence the work reported in this paper.

Acknowledgments

The authors thank Drs. K. Nagaishi of Marine Works Japan Ltd. and K-C. Shin of the Research Institute for Humanity and Nature for assistance with the isotopic and chemical analyses. This work was funded by KAKENHI grants (numbers JP26870418 and JP16H04066) from the Japan Society for the Promotion of Science. We also thank the associate editor, Zhonghui Liu, and two anonymous reviewers for constructive comments and suggestions, which improved the quality of our logic and interpretations.

Appendix A

See Tables A.1 and A.2.

Table A.1
Locations of sampling sites and grain size statistics of samples after grain-size separation.

Sample No.	Sampling location		Grain size (μm)			
	latitude (°N)	longitude (°E)	10th percentile	Median	90th percentile	Mode
1	31.2801	131.0674	1.4	6.6	22.0	9.2
2	31.4773	131.0453	1.4	5.6	17.8	7.1
3	31.4770	131.0459	1.7	7.7	23.9	9.8
4	31.6226	131.3505	1.2	5.2	14.6	7.0
5	31.6225	131.3505	1.0	4.3	13.4	5.7
6	31.9524	131.3661	1.3	5.2	16.1	6.8
7	31.9525	131.3659	1.3	5.2	15.1	6.9
8	32.0832	131.4138	1.2	5.6	16.7	7.2
9	32.0831	131.4138	1.2	5.2	14.9	6.8
10	32.2619	131.5727	1.2	6.6	33.1	7.6
11	32.2619	131.5727	1.2	6.2	29.2	7.4
12	32.5654	131.5811	1.4	6.1	20.0	7.2
13	32.5655	131.5809	1.4	6.3	19.9	7.5
14	32.9538	131.8503	1.1	5.2	20.5	6.8
15	32.9538	131.8503	1.1	5.2	21.8	6.5
16	33.0811	131.8394	1.0	3.7	15.5	3.7
17	33.0813	131.8390	1.0	4.2	18.5	4.1
18	33.1968	131.6838	1.2	5.1	17.8	6.8
19	33.1968	131.6838	1.3	5.5	19.8	7.0
20	33.2030	131.6051	1.3	5.4	19.8	6.2
21	33.2034	131.6062	1.2	5.5	18.5	7.3
22	33.5958	131.1779	1.3	5.2	17.8	5.9
23	33.5987	131.1777	1.4	5.8	21.6	6.3
24	33.5085	132.5511	1.6	6.5	17.8	8.4
25	33.5075	132.5518	1.5	6.5	19.9	8.0
26	33.5082	132.5516	1.6	6.2	16.0	7.9
27	32.8706	132.9473	1.0	4.4	17.5	5.2
28	32.9925	132.9234	1.0	4.9	19.1	6.3
29	32.9927	132.9232	1.1	4.5	15.2	5.6
30	32.9749	132.9441	1.0	3.7	10.7	4.7
31	33.3915	133.2627	1.2	4.3	12.5	5.5
32	33.3858	133.2769	1.2	5.1	23.0	5.6
33	33.4943	133.4509	1.3	5.8	17.6	7.4
34	33.4959	133.4457	1.4	6.1	19.4	7.8
35	33.4961	133.4453	1.4	6.0	17.7	7.6
36	33.9407	134.5784	0.9	4.1	10.8	5.7
37	33.9399	134.5782	1.1	3.6	9.0	4.5
38	34.1044	134.4376	2.0	7.0	16.2	8.4
39	34.1037	134.4373	2.3	7.9	17.9	9.4
40	34.9058	135.7137	1.0	3.4	11.0	3.7
41	34.9058	135.7137	1.4	5.5	15.8	6.3
42	34.9204	135.7506	1.0	3.3	8.8	3.8
43	34.8744	135.7326	1.8	7.7	20.8	10.0
44	34.8739	135.7331	1.2	4.5	15.9	4.4
45	34.8739	135.7331	1.5	6.2	20.3	7.3
46	34.8262	135.6420	1.1	4.0	11.6	4.4
47	34.8262	135.6420	1.1	4.0	11.4	4.5
48	34.8262	135.6420	1.1	3.7	10.8	4.1
49	34.8262	135.6420	1.1	4.3	11.4	5.1
50	34.2507	135.3405	1.1	4.1	13.0	4.6
51	34.2507	135.3405	1.2	4.4	14.9	4.6
52	33.9023	135.1916	1.0	3.9	10.0	5.6
53	33.5887	135.4494	1.1	4.6	14.9	5.2
54	33.5887	135.4494	0.9	3.9	10.5	5.4
55	33.7332	135.9752	1.1	4.1	10.9	5.7
56	33.7349	135.9742	1.0	4.5	12.1	6.6
57	34.4837	136.6838	2.0	10.0	25.9	13.5
58	34.4831	136.6833	1.4	6.4	17.3	8.9
59	34.5265	136.5751	1.6	6.4	15.8	8.0
60	34.5263	136.5750	1.7	6.7	17.1	8.7
61	34.6393	136.3365	1.2	4.9	13.0	6.5
62	34.6382	136.3364	1.2	5.1	13.0	6.9
63	34.8514	136.4101	1.7	7.8	22.9	10.0
64	34.8511	136.4094	1.6	7.2	21.0	9.5

(*continued on next page*)

Table A.1 (*continued*)

Sample No.	Sampling location		Grain size (μm)			
	latitude (°N)	longitude (°E)	10th percentile	Median	90th percentile	Mode
65	35.1441	136.5142	0.9	3.9	11.1	5.7
66	35.1442	136.5153	1.0	3.9	11.1	5.5
67	35.3939	136.6432	1.2	5.5	17.0	7.5
68	35.3945	136.6429	1.2	5.7	18.3	9.3
69	35.4098	136.7066	1.3	6.7	20.5	10.4
70	35.4092	136.7059	1.1	4.7	14.4	6.4
71	35.3692	136.7711	1.1	4.7	14.4	6.1
72	35.3695	136.7732	1.1	4.6	13.1	5.7
73	35.2101	136.8866	1.1	4.3	12.9	5.5
74	35.2102	136.8863	1.2	4.9	14.3	6.5
75	34.9366	137.1411	n.a.	n.a.	n.a.	n.a.
76	34.9365	137.1411	1.7	8.4	24.2	12.4
77	34.9364	137.1414	1.8	8.8	25.1	12.6
78	34.8169	137.4315	1.4	6.5	19.1	8.9
79	34.7394	137.8098	1.1	4.8	14.9	6.2
80	34.7422	137.8124	1.0	4.0	11.8	5.6
81	34.8164	138.2364	1.0	3.5	9.6	5.1
82	34.8184	138.2324	0.7	2.3	8.3	1.9
83	34.8189	138.2336	0.8	2.5	8.1	2.2
84	34.9500	138.3789	1.0	3.7	10.0	5.1
85	34.9506	138.3796	1.0	3.5	9.4	4.9
86	35.1392	138.6320	1.2	4.9	12.1	6.5
87	35.1383	138.6326	1.2	4.6	12.3	5.8
88	35.1383	138.6326	1.3	5.2	13.6	6.7
89	35.0216	138.9393	1.2	4.2	11.0	5.7
90	35.0213	138.9389	1.1	3.8	10.4	5.0
91	35.0863	138.9051	1.3	4.4	11.9	5.8
92	35.2678	139.1749	1.1	4.2	12.4	5.4
93	35.4444	139.3727	1.1	4.1	11.7	5.5
94	35.4458	139.3710	1.8	9.9	25.1	14.0
95	35.4497	139.3718	0.9	3.8	17.6	2.7
96	35.6531	139.4787	1.2	5.7	20.3	10.9
97	35.6532	139.4785	1.0	3.8	11.5	4.9
98	35.8313	139.6134	1.1	4.5	14.4	5.3
99	35.8313	139.6134	1.2	4.5	13.0	5.2
100	35.8313	139.6134	1.0	4.5	12.0	6.4
101	35.9269	139.9633	1.2	5.0	13.4	6.5
102	35.9269	139.9633	1.3	5.3	14.8	6.6

Table A.2
Results of principal component analysis derived from the isotope ratios of sediments from watersheds where J-A-i, J-A-o, Cr-A, Q-V, Cr-P, or Cr-M occupy more than half of the watershed area.

Principal component	Loadings					Eigenvalues	Contribution (%)
	$^{87}Sr/^{86}Sr$	$^{143}Nd/^{144}Nd$	$^{206}Pb/^{204}Pb$	$^{207}Pb/^{204}Pb$	$^{208}Pb/^{204}Pb$		
PC1	0.433	−0.430	0.422	0.483	0.466	4.078	81.6
PC2	−0.433	0.566	0.646	0.075	0.263	0.599	12.0
PC3	0.730	0.457	0.271	−0.077	−0.422	0.220	4.4
PC4	0.274	0.114	−0.103	−0.686	0.656	0.076	1.5
PC5	−0.128	−0.523	0.567	−0.533	−0.324	0.027	0.5

References

Asahara, Y., 1999. $^{87}Sr/^{86}Sr$ variation in north Pacific sediments: a record of the Milankovitch cycle in the past 3 million years. Earth Planet. Sci. Lett. 171, 453–464.

Asahara, Y., Tanaka, T., Kamioka, H., Nishimura, A., 1995. Asian continental nature of $^{87}Sr/^{86}Sr$ ratios in north central Pacific sediments. Earth Planet. Sci. Lett. 133, 105–116.

Bentahila, Y., Othman, D.B., Luck, J.-M., 2008. Strontium, lead and zinc isotopes in marine cores as tracers of sedimentary provenance: A case study around Taiwan orogen. Chem. Geol. 248, 62–82.

Aubert, D., Stille, P., Probst, A., 2001. REE fractionation during granite weathering and removal by waters and suspended loads: Sr and Nd isotopic evidence. Geochim. Cosmochim. Acta 65, 387–406.

Blum, J.D., Erel, Y., 1997. Rb-Sr isotope systematics of a granitic soil chronosequence: The importance of biotite weathering. Geochim. Cosmochim. Acta 61, 3193–3204.

Brown, M., 2010. Paired metamorphic belts revisited. Gondwana Res. 18, 46–59.

Chen, J., Li, G., Yang, J., Rao, W., Lu, H., Balsam, W., Sun, Y., Ji, J., 2007. Nd and Sr isotopic characteristics of Chinese deserts: Implications for the provenances of Asian dust. Geochim. Cosmochim. Acta 71, 3904–3914.

Dou, Y., Yang, S., Liu, Z., Zhi, X., Yu, H., Berne, S., 2012. Sr–Nd isotopic constraints on terrigenous sediment provenances and Kuroshio Current variability in the Okinawa Trough during the late Quaternary. Palaeogeogr. Palaeoclimatol. Palaeoecol. 365–366, 38–47.

Ehlert, C., Frank, M., 2011. Current transport versus continental inputs in the eastern Indian Ocean: Radiogenic isotope signatures of clay size sediments. Geochem. Geophys. Geosyst. 12, Q06017.

Feng, J.-L., Zhu, L.-P., Zhen, X.-L., Hu, Z.-G., 2009. Sr–Nd isotopic constraints on terrigenous sediment provenances and Kuroshio Current variability in the Okinawa Trough during the late Quaternary. Geochem. J. 43, 123–131.

Ferguson, W.S., Griffin, J., Goldberg, E.D., 1970. Atmospheric dusts from the north Pacific–a short note on a long-range eolian transport. J. Geophys. Res. 75, 1137–1139.

Franzese, A.M., Hemming, S.R., Goldstein, S.L., 2009. Use of strontium isotopes in detrital sediments to constrain the glacial position of the Agulhas Retroflection. Paleoceanography 24, PA2217.

Franzese, A.M., Hemming, S.R., Goldstein, S.L., Anderson, R.F., 2006. Reduced Agulhas Leakage during the Last Glacial Maximum inferred from an integrated provenance and flux study. Earth Planet. Sci. Lett. 250, 72–88.
Garcia, D., Ravenne, C., Maréchal, B., Moutte, J., 2004. Geochemical variability induced by entrainment sorting: quantified signals for provenance analysis. Sed. Geol. 171, 113–128.
Garcon, M., Chauvel, C., France-Lanord, C., Limonta, M., Garzanti, E., 2013. Removing the "heavy mineral effect" to obtain a new Pb isotopic value for the upper crust. Geochem. Geophys. Geosyst. 14, 3324–3333.
Garzanti, E., Andò, S., Vezzoli, G., 2008. Settling equivalence of detrital minerals and grain-size dependence of sediment composition. Earth Planet. Sci. Lett. 273, 138–151.
Geological Survey of Japan, AIST (Eds.), 2015. Seamless digital geological map of Japan 1: 200,000. May 29, 2015 version. Geological Survey of Japan, National Institute of Advanced Industrial Science and Technology, Tsukuba, Japan.
GEOROC (http://georoc.mpch-mainz.gwdg.de/georoc/). Last accessed in October 11, 2019.
Grousset, F.E., Biscaye, P.E., 2005. Tracing dust sources and transport patterns using Sr, Nd and Pb isotopes. Chem. Geol. 222, 149–167.
Grousset, F.E., Biscaye, P.E., Revel, M., Petit, J.-R., Pye, K., Joussaume, S., Jouzel, J., 1992. Antarctic (Dome C) ice-core dust at 18 k.y. B.P.: Isotopic constraints on origins. Earth Planet. Sci. Lett. 111, 175–182.
Hovan, S.A., Rea, D.K., Pisias, N.G., 1991. Late Pleistocene continental climate and oceanic variability recorded in northwest Pacific sediments. Paleoceanography 6, 349–370.
Honjo, S., Manganini, S.J., Poppe, L.J., 1982. Sedimentation of lithogenic particles in the deep ocean. Mar. Geol. 50, 199–220.
Hunter,, 1998. Intracrustal controls on the coexistence of tholeiitic and calc-alkaline magma series at Aso volcano, SW Japan. J. Petrol. 39, 1255–1284.
Huang, H., 2011. Time lag between reduction of sediment supply and coastal erosion. Int. J. Sedim. Res. 26, 27–35.
Isozaki, Y., Itaya, T., 1990. Chronology of Sanbagawa metamorphism. J. Metamorph. Geol. 8, 401–411.
Jomori, et al., 2013. Spatial distribution of $^{87}Sr/^{86}Sr$ ratios of stream sediments in Shikoku Island and the Kii Peninsula, Southwest Japan. Geochem. J. 47, 321–335.
Jones, C.E., Halliday, A.N., Rea, D.K., Owen, R.M., 1994. Neodymium isotopic variations in North Pacific modern silicate sediment and the insignificance of detrital REE contributions to seawater. Earth Planet. Sci. Lett. 127, 55–66.
Jones, C.E., Halliday, A.N., Rea, D.K., Owen, R.M., 2000. Eolian inputs of lead to the North Pacific. Geochim. Cosmochim. Acta 64, 1405–1416.
Kagami, H., Iizumi, S., Tainosho, Y., Owada, M., 1992. Spatial variations of Sr and Nd isotope ratios of Cretaceous-Paleogene granitoid rocks, Southwest Japan Arc. Contrib. Miner. Petrol. 112, 165–177.
Kamata, H., Kodama, K., 1994. Tectonics of an arc-arc junction: an example from Kyushu Island at the junction of the Southwest Japan Arc and the Ryukyu Arc. Tectonophysics 233, 69–81.
Kawahata, H., Ohshima, H., 2002. Small latitudinal shift in the Kuroshio Extension (Central Pacific) during glacial times: evidence from pollen transport. Quat. Sci. Rev. 21, 1705–1717.
Korup, O., Hayakawa, Y., Codilean, A.T., Matsushi, Y., Saito, H., Oguchi, T., Matsuzaki, H., 2014. Japan's sediment flux to the Pacific Ocean revisited. Earth Sci. Rev. 135, 1–16.
Kusuhashi, N., Yamaji, A., 2001. Miocene tectonics of SW Japan as inferred from the Kuma Group, Shikoku. J. Geol. Soc. Japan 107, 26–40.
Lamy, F., Hebbeln, D., Röhl, U., Wefer, G., 2001. Holocene rain fall variability in southern Chile: a marine record of latitudinal shifts of the Southern Westerlies. Earth Planet. Sci. Lett. 185, 369–382.
Li, G., Pettke, T., Chen, J., 2011. Increasing Nd isotopic ratio of Asian dust indicates progressive uplift of the north Tibetan Plateau since the middle Miocene. Geology 39, 199–202.
Matsuoka, A., 1992. Jurassic-Early Cretaceous tectonic evolution of the Southern Chichibu terrane, southwest Japan. Palaeogeogr. Palaeoclimatol. Palaeoecol. 96, 71–88.
Mayer, I., Davies, G.R., Stuut, J.-B.W., 2011. Grain size control on Sr-Nd isotope provenance studies and impact on paleoclimate reconstructions: An example from deep-sea sediments offshore NW Africa. Geochem. Geophys. Geosyst. 12, Q03005.
Meng, X., Liu, Y., Shi, X., Du, D., 2008. Nd and Sr isotopic compositions of sediments from the Yellow and Yangtze Rivers: Implications for partitioning tectonic terranes and crust weathering of the Central and Southeast China. Front Earth Sci. China 2, 418–426.
Miyashiro, A., 1961. Evolution of metamorphic belts. J. Petrol. 2, 277–311.
Morton, A.C., Hallsworth, C.R., 1999. Processes controlling the composition of heavy mineral assemblages in sandstones. Sed. Geol. 124, 3–29.
Nagai, T., Takahashi, M., Hirahara, Y., Shuto, K., 2004. Sr-Nd isotopic compositions of volcanic rocks from Fuji, Komitake and Ashitaka volcanoes, Central Japan. Proc. Instit. Nat. Sci., Nihon University 39, 205–215.
Nakae, S., 2000. Regional correlation of the Jurassic accretionary complex in the Inner Zone of Southwest Japan. Memoirs Geol. Soc. Japan 55, 73–98.
Nakai, S., Halliday, A.N., Rea, D.K., 1993. Provenance of dust in the Pacific Ocean. Earth Planet. Sci. Lett. 119, 143–157.
Nakajima, T., 1994. The Ryoke plutonometamorphic belt: crustal section of the Cretaceous Eurasian continental margin. Lithos 33, 51–66.
Nakano, T., Yokoo, Y., Nishikawa, M., Koyanagi, H., 2004. Regional Sr-Nd isotopic ratios of soil minerals in northern China as Asian dust fingerprints. Atmos. Environ. 38, 3061–3067.
Okamoto, K., Maruyama, S., Isozaki, Y., 2000. Accretionary complex origin of the Sanbagawa, high P/T metamorphic rocks, Central Shikoku, Japan–Layer-parallel shortening structure and greenstone geochemistry. J. Geol. Soc. Japan 106, 70–86.
Okano, O., Sato, T., Kagami, H., 2000. Rb-Sr and Sm-Nd isotopic studies of mafic igneous rocks from the Ryoke plutono-metamorphic belt in the Setouchi area, Southwest Japan: implications for the genesis and thermal history. The Island Arc 9, 21–36.
Olivarez, A.M., Owen, R.M., Rea, D.K., 1991. Geochemistry of eolian dust in Pacific pelagic sediments: Implications for paleoclimatic interpretations. Geochim. Cosmochim. Acta 55, 2147–2158.
Pettke, T., Halliday, A.N., Hall, C.M., Rea, D.K., 2000. Dust production and deposition in Asia and the north Pacific Ocean over the past 12Myr. Earth Planet. Sci. Lett. 178, 397–413.
T. Pettke A.N. Halliday D.K. Rea Cenozoic evolution of Asian climate and sources of Pacific seawater Pb and Nd derived from eolian dust of sediment core LL44-GPC3 Paleoceanography 17 2002 3–1–3-13.
Pickering, K.T., Underwood, M.B., Taira, A., 1992. Open-ocean to trench turbidity-current flow in the Nankai Trough: Flow collapse and reflection. Geology 20, 1099–1102.
R Core Team, 2019. R: A language and environment for statistical computing. R Foundation for Statistical Computing, Vienna, Austria. https://www.R-project.org/.
Rea, D.K., Leinen, M., Janecek, T.R., 1985. Geologic approach to the long-term history of atmospheric circulation. Science 227, 721–725.
Rea, D.K., Snoeckx, H., Joseph, L.H., 1998. Late Cenozoic eolian deposition in the North Pacific: Asian drying, Tibetan uplift, and cooling of the northern hemisphere. Paleoceanography 13, 215–224.
Saitoh, Y., 2014. Grain-size distribution of the late Cenozoic hemipelagic mud from C0011. In: Henry, P., Kanamatsu, T., Moe, K., and the Expedition 333 Scientists, Proceedings of the Integrated Ocean Drilling Program 333. Integrated Ocean Drilling Program Management International, Inc., Tokyo, MS 333-203.
Saitoh, Y., Ishikawa, T., Tanimizu, M., Murayama, M., Ujiie, Y., Yamamoto, Y., Ujiie, K., Kanamatsu, T., 2015. Sr, Nd, and Pb isotope compositions of hemipelagic sediment in the Shikoku Basin: Implications for sediment transport by the Kuroshio and Philippine Sea plate motion in the late Cenozoic. Earth Planet. Sci. Lett. 421, 47–57.
Sakashima, T., Terada, K., Takeshita, T., Sano, Y., 2003. Large-scale displacement along the Median Tectonic Line, Japan: evidence from SHRIMP zircon U-Pb dating of granites and gneisses from the South Kitakami and paleo-Ryoke belts. J. Asian Earth Sci. 21, 1019–1039.
Scheidegger, K.F., Krissek, L.A., 1982. Dispersal and deposition of eolian and fluvial sediments off Peru and northern Chilie. GSA Bulletin 93, 150–162.
Schindlbeck, J.C., Jegen, M., Freundt, A., Kutterolf, S., Straub, S.M., Mleneck-Vautravers, M.J., McManus, J.F., 2018. 100-kyr cyclicity in volcanic ash emplacement: evidence from a 1.1 Myr tephra record from the, NW Pacific. Scientific Reports 8, 4440.
Shibata, H., 1967. Geology of the Miocene Ichishi Group. J. Geol. Soc. Japan 73, 337–346.
Shibata, T., Suzuki, J., Yoshikawa, M., Kobayashi, T., Miki, D., Takemura, K., 2013. Geochemical and Sr-Nd-Pb isotopic constraints on the origin and magmatic evolution of Quaternary Lavas of Sakurajima volcano, Southern Kyushu Island, Japan. Bull. Volcanol. Soc. Japan 58, 43–58.
Stumpf, R., Frank, M., Schönfeld, J., Haley, B.A., 2011. Climatically driven changes in sediment supply on the SW Iberian shelf since the Last Glacial Maximum. Earth Planet. Sci. Lett. 312, 80–90.
Sugiyama, Y., 1994. Neotectonics of Southwest Japan due to the right-oblique subduction of the Philippine Sea plate. Geofísica Internacional 33, 53–76.
Sun, J., 2005. Nd and Sr isotopic variations in Chinese eolian deposits during the past 8 Ma: Implications for provenance change. Earth Planet. Sci. Lett. 240, 454–466.
Sun, J., Zhu, X., 2010. Temporal variations in Pb isotopes and trace element concentrations within Chinese eolian deposits during the past 8 Ma: Implications for provenance change. Earth Planet. Sci. Lett. 290, 438–447.
Tailor, R.N., Nesbitt, R.W., 1998. Isotopic characteristics of subduction fluids in an intra-oceanic setting, Izu-Bonin Arc, Japan. Earth Planet. Sci. Lett. 164, 79–98.
Taira, A., 2001. Tectonic evolution of the Japanese island arc system. Annu. Rev. Earth Planet. Sci. 29, 109–134.
Taira, A., Niitsuma, N., 1986. Turbidite sedimentation in the Nankai Trough as interpreted from magnetic fabric, grain size, and detrital modal analyses. DSDP Initial Reports 87, 611–632.
Tanaka, T., Togashi, S., Kamioka, H., Amakawa, H., Kagami, H., Hamamoto, T., Yuhara, M., Orihashi, Y., Yoneda, S., Shimizu, H., Kunimaru, T., Takahashi, K., Yanagi, T., Nakano, T., Fujimaki, H., Shinjo, R., Asahara, Y., Tanimizu, M., Dragusanu, C., 2000. JNdi-1: a neodymium isotopic reference in consistency with LaJolla neodymium. Chem. Geol. 168, 279–281.
Tanimizu, M., Ishikawa, T., 2006. Development of rapid and precise Pb isotope analytical techniques using MC-ICP-MS and new results for GSJ rock reference samples. Geochem. J. 40, 121–133.
Tatsumi, Y., 1989. Migration of fluid phases and genesis of basalt magmas in subduction zones. J. Geophys. Res. 94, 4697–4707.
Tazawa, J., 2000. The Palaeozoic of the Hida Gaien, South Kitakami and Kurosegawa belts: Correlation and tectonic history. Memoirs Geol. Soc. Japan 56, 39–52.
Terakado, Y., Shimizu, H., Masuda, A., 1988. Nd and Sr isotopic variations in acidic rocks formed under a peculiar tectonic environment in Miocene Southwest Japan. Contrib. Mineral. Petrol. 99, 1–10.
Uematsu, M., Duce, R.A., Prospero, J.M., Chen, L., Merrill, J.T., McDonald, R.L., 1983. Transport of mineral aerosol from Asia over the North Pacific Ocean. J. Geophys. Res. 88, 5343–5352.
Underwood, M.B., Furgusson, C.L., 2005. Late Cenozoic evolution of the Nankai trench-slope system: evidence from sand petrography and clay mineralogy. In: Hodgson, D. M., Flint, S.S. (Eds.), Submarine Slope Systems: Processes and Products. Geological Society, London, Special Publications 244, pp. 133–129.
Uno, M., Iwamori, H., Nakamura, H., Yokoyama, T., Ishikawa, T., Tanimizu, M., 2014.

Elemental transport upon hydration of basic schists during regional metamorphism: geochemical evidence from the Sanbagawa metamorphic belt, Japan. Geochem. J. 48, 29–49.
Uyeda, S., Miyashiro, A., 1974. Plate tectonics and the Japanese Islands: A synthesis. Geol. Soc. Am. Bull. 85, 1159–1170.
van der Lubbe, H.J.L., Frank, M., Tjallingii, R., Schneider, R.R., 2016. Neodymium isotope constraints on provenance, dispersal, and climate-driven supply of Zambezi sediments along the Mozambique Margin during the past ~45,000 years. Geochem. Geophys. Geosyst. 17, 181–198.
Wang, H., Saito, Y., Zhang, Y., Bi, N., Sun, X., Yang, Z., 2011. Recent changes of sediment flux to the western Pacific Ocean from major rivers in East and Southeast Asia. Earth Sci. Rev. 108, 80–100.
Windom, H.L., 1969. Atmospheric dust records in permanent snowfield: implications to marine sedimentation. Geol. Soc. Am. Bull. 80, 761–782.
Yang, S., Jiang, S., Ling, H., Xia, X., Sun, M., Wang, D., 2007. Sr-Nd isotopic compositions of the Changjiang sediments: Implications for tracing sediment sources. Sci. China, Ser. D Earth Sci. 50, 1556–1565.
Yoshida, F., 1987. Planktonic foraminifera from the Miocene Awa Group, Mie Prefecture, central Japan. Bull. Geol. Survey Japan 38, 473–483.
Zhang, W., Chen, J., Ji, J., Li, G., 2016. Evolving flux of Asian dust in the North Pacific Ocean since the late Oligocene. Aeolian Res. 23, 11–20.
Zheng, X., Li, A., Kao, S., Gong, X., Frank, M., Kuhn, G., Cai, W., Yan, H., Wan, S., Zhang, H., Jiang, F., Hathorne, D., Chen, Z., Hu, B., 2016. Synchronicity of Kuroshio Current and climate system variability since the Last Glacial Maximum. Earth Planet. Sci. Lett. 452, 247–257.